Universidad Autónoma de Nuevo León

Facultad de Ingeniería Mecánica y Eléctrica

Subdirección de Estudios de Posgrado

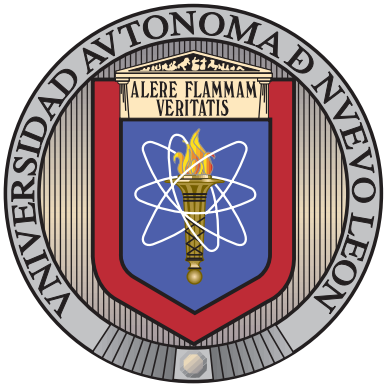

Analysis and modeling of micro turbojets: a comprehensive model based on multiphysics principles

por

Jose Francisco Villarreal Valderrama

como requisito parcial para obtener el grado de

maestría en ingeniería aeronáutica

con orientacion en Dinámica de Vuelo

Junio de 2019

Universidad Autónoma de Nuevo León

Facultad de Ingeniería Mecánica y Eléctrica

Subdirección de Estudios de Posgrado

Analysis and modeling of micro turbojets: a comprehensive model based on multiphysics principles

por

Jose Francisco Villarreal Valderrama

como requisito parcial para obtener el grado de

maestría en ingeniería aeronáutica

con orientacion en Dinámica de Vuelo

Junio de 2019

Universidad Autónoma de Nuevo León

Facultad de Ingeniería Mecánica y Eléctrica

Subdirección de Estudios de Posgrado

Los miembros del Comité de Tesis recomendamos que la Tesis «Análisis y modelado de micro turborreactores: Un modelo comprensivo basado en principios multifísicos», realizada por el alumno Jose Francisco Villarreal Valderrama, con número de matrícula 1565437, sea aceptada para su defensa como requisito parcial para obtener el grado de Maestría en Ingeniería Aeronáutica con orientacion en Dinámica de Vuelo.

El Comité de Tesis

Dr. Luis Antonio Amézquita Brooks

Asesor

Dr. Eduardo Liceaga Castro

Revisor

Dr. Octavio García Salazar

Revisor

Vo. Bo.

Dr. Simón Martínez Martínez

Subdirección de Estudios de Posgrado

SUBDIRECCIÓN DE ESTUDIOS DE POSGRADO
FACULTAD DE INGENIERÍA MECÁNICA Y ELÉCTRICA
U.A.N.L.
FIME

San Nicolás de los Garza, Nuevo León, junio de 2019

A mis padres,

José Francisco Villarreal Lozano y Virginia Valderrama Almanza,

los cuales han sido un gran ejemplo y mi motivación para seguir adelante.

Contents

List of Figures

List of Tables

Agradecimientos

En la presente quiero agradecer a la Facultad de Ingeniería Mecánica y Eléctrica, por medio de la cual se me otorgó acceso a las instalaciones del Centro de Investigación e Innovación en Ingeniería Aeronáutica; sin las cuales esta tesis no hubiera sido posible. También me gustaría dar mi agradecimiento a CONACyT, por brindarme el apoyo para seguir con mis estudios de posgrado durante estos dos años.

Adicionalmente, un agradecimiento especial a mis mentores Luis Amézquita, Eduardo Liceaga, Daniel Librado y Octavio García, por haberme aconsejado y orientado a lo largo de este trayecto.

Mi familia merece un gran agradecimiento por el apoyo y paciencia que me brindaron durante mis estudios.

Resumen

Jose Francisco Villarreal Valderrama.

Candidate to obtain the degree of *Maestría en Ingeniería Aeronáutica con orientacion en Dinámica de Vuelo.*

Universidad Autónoma de Nuevo León.

Facultad de Ingeniería Mecánica y Eléctrica.

Title of the study: Analysis and modeling of micro turbojets: a comprehensive model based on multiphysics principles.

Number of pages: 71.

Objectives and study method: The development of accurate models to represent turbojet performance is presented as a tool to meet the growing need for reliable unmanned aerial vehicle propulsion systems. In the present, the objective is to develop a model to incorporate different physical systems to estimate the most important engine variables at different operating conditions. The experimental measurements are designed to simulate flight conditions up to 130 km /hr in a wind tunnel.

Intensive engine tests and the design of wind tunnel instrumentation to measure the undisturbed wind tunnel flow speed. During the tests, pressures and temperatures of each engine component, flow velocity, rotational speed of the shaft, thrust

and fuel flow were measured.

CONTRIBUTIONS AND CONCLUSIONS: The model was developed in the context of block diagrams, in which each block corresponds to a motor station and the lines are auxiliary for the visualization of the relationships between the motor variables. The equations that govern the system are defined according to fundamental physical principles. The comparison among the results obtained by applying the conventional theory, the experimental results and the model here developed are presented.

The model proposed was validated through extensive tests. The engine was submitted up to 130 km/hr wind speed. The performance registered by the model here obtained for each operating condition tested showed an error below the 6.24

Firma del asesor: _____

Dr. Luis Antonio Amézquita Brooks

Nomenclature

Table 1: Variables and parameters nomenclature

γ	Specific heat ratio
η	Efficiency
θ	Unknown coefficient vector
π	Component pressure ratio
ρ	Density (Kg/m^3)
τ	Component temperature ratio
A	Cross sectional area (m^2)
a	Sound speed (m/s)
b	Polinomial coefficients
C_D	Aerodynamic drag coefficient
C_P	Constant pressure specific heat ($\frac{J}{KgK}$)
D	Aerodynamic drag (N)
e	Polytropic efficiency
F	Thrust (N)
f	Fuel mass flow to air mass flow ratio
F_l	Load celll pre-load (N)
F_m	Load cell measured force (N)
h	Enthalpy (J/Kg)
h^o	Molar enthalpy ($J/mole$)
J	Cost function

M	Mach speed
M_m	Molecular mass (Kg/mol)
$\dot{m}$	Mass flow (Kg/s)
$\dot{m}$	Fuel mass flow (Kg/s)
N	Shafts speed (RPM)
o	Independent variable measurement
P	Pressure (KPa)
P_l	Applied pre-load (N)
PCI	Lower specific heating value (J/Kg)
r	Radius (m)
t	Time (s)
T	Temperature (^oK)
u	Number of tests
V	Wind speed (m/s)
W	Work (J)
X	Independent variable measurements vector
Y	Dependent variable measurements vector
y	Dependent variable measurement

Table 2: Subindex nomenclature

α	Arbitrary wind tunnel section
β	Test chamber wind tunnel section
λ	Turbine inlet to ambient temperatures ratio
∞	Free stream properties
0	Turbojet inlet properties
1	Difusser exit properties
2	Compressor exit properties
3	Combustion chamber exit properties
4	Turbine exit properties
5	Exhaust gas properties
b	Combustion chamber section
c	Compressor section
cr	Combustion reactives
D	Dynamic
d	Difusser section
e	Component exit conditions
f	Formation
I	Ideal
i	Component inlet conditions
j	Amount of data samples
k	Polynomial dimension
n	Nozzle section
p	Combustion products
R	Reference conditions
r	Stagnation properties
S	Static
T	Total
t	Turbine section
x	Arbitrary turbojet component

Chapter 1

Justification

The majority of the parameter estimation of dynamical systems methods rely on a proposed structure. Regardless of the precision of the parameters estimation, if the structure is not appropiate, the estimation model rapidly diverges from the experimental conditions. A source of this divergence are the un-modelled non-linearities [26]. A model with a structure that allows covering multiphysical phenomena would allow to:

- Improve current fault detection systems.
- Simplify performance analysis.
- Evaluate performance under flight conditions that would be unsafe to experimentally test.
- Improve the control systems performance.
- Enhace engine optimization.

  The aim of this work is to satisfy the above characteristics through a novel model.

Chapter 2

Hypothesis, objectives and methodology

2.1 Hypothesis

The combination of aerothermal models with turbomachinery principles provides a more representative dynamical structure for micro-turbojet engines. Thus, improving the prediction of the performance parameters at wider operating conditions.

2.2 Objective

To obtain a model that captures the steady state operating conditions of a micro-turbojet in flight conditions. The flight conditions are emulated by incorporating the turbo engine in a wind tunnel. This situation corresponds to a small aircraft flight. As follows, physical based principles and experimental tests on wind tunnel facilities are extensively applied.

2.3 Identification process development

The process required to accomplish the main objective involves different fundamental steps:

- Develop the necessary instrumentation.
- Improve the measurements through signal processing and compute the engine drag coefficient.
- Carry out tests to simulate flight conditions up to 130 km / hr and calibrate the thrust measurements with the computed aerodynamic drag.
- Determine the fundamental structure of the model according to physical laws, experimental observations and available research information.
- Calculate the parameters of the structure based on experiments.
- Validate model accuracy at different operating conditions with further experimental tests.

Chapter 3

Introduction

Multiphysics models have acquired recent attention to model processes with different simultaneous interacting physical properties. Multiphysic processes are characterized the variable coupling of diferent physical phenomena, which occur simultaneously. The development of a multiphysic model requires previous knowledge of the individual interacting systems and the relationship among the subsystem interactions. Turbojets are an example of multiphysic systems with multiple processes taking place simultaneously , the main mechanisms are heat transfer, pneumatic processes and mechanical interactions [46].

Jet engine modelling has been controversial due to its complexicity and limited sensor information during flight [39]. The earliest performance models were based on statistical representations. These estimation methods require large data bases and do not provide information on the transient behaviour of the variables [35]. Conventional models are either data-based, such as transfer functions or physics-based, such as thermodynamic models.

Physics-based models are developed through thermodynamic laws. Early thermodynamic models were valid only for narrow operation points [29] due to the asumption that the efficiency parameters could be modeled by static coefficients [24]. Some alternatives to improve the models performance were the inclusion of

the main source of perturbations, such as environmental conditions [11], and developing simple and transparent models to capture the engine physics [12]. In 1996, models based on mass and momentum balance were tested experimentally for small operation ranges in an industrial gas turbine [13]. These models lose accuracy at high thermal states [14] and are valid only for narrow operation points with slow accelerations/decelerations [25]. A common error source in these models is the shaft speed dynamics, which is either not captured by conventional thermodynamic models [58]. Aerothermal models were presented to handle some of the nonlinearities in jet engines and are used for health estimation applications by comparing measured thermodynamic variables and model baseline estimations [39]. As microturbojets usually operate at 20 times the jet engine operation speed, conventional models have presented unrealistic performance parameters due to operating Reynolds number, tip clearances, boundary layers and profile losses differences [9].

Data-based models are black box approaches, which have been also considered for turbojet variables estimation. These models have been proposed as an alternative to conventional thermodynamic models, which lose accuracy at high thermal states [14]. Earlier attempts were based on transfer function identification through least squares response estimation to pseudo random binary sequence (PRBS) inputs. Although this method leads to unrealistic pole locations [29], it provided useful approaches for black box engine modelling.

3.1 Models applications

The development of improved estimation models is of great interest for aerospace and energy engineering. Comparing the computed performance maps, any engine modification can be evaluated in terms of efficiency and operational safety [68]. Component degradation can be detected by comparing model baseline estimations to real engine measurements, thus maintenance can be applied in terms of actual degradation instead of flight time [65]. Failure detection algorithms have been also developed to

ensure safe operation, these algorithms are based on aerothermal models combined with optimization techniques to match engine and model health parameters [64]. Models with high accuracy can be used to provide engine performance information for non-conventional flight conditions, which may be unsafe to test experimentally with previous engine information [2]. Neural network models have been implemented to optimize engine operation, leading to reduced fuel consumption during normal operation [22]. The development of unmanned aerial vehicles demands nonlinear models to improve control schemes of microturbines, due to its wider operation regimes and flight conditions [4]. This shows that engine modelling is fundamental for many applications and although the engine efficiency and health parameter computation has been widely analyzed, few insight on developing a fundamental engine structure has been presented.

3.2 Physics-based estimation

As physics-based estimation is the most attractive approach for health condition diagnosis [16], some alternatives have been presented to expand the model capabilities for wider operating points. White box modelling is a common approach, as there is enough knowledge available about the physics of the turbojet gas generator section.

A common approach for improving the model estimation is to extract data from performance maps. Performance maps are graphical representations of the turbojet performance, which consist in a pressure or efficiency axis and a flow axis. In these maps, lines representing a constant speed condition across the operating condition are used. These lines are used to match the engine thermal state and external operating conditions to performance parameters. As piecewise linear functions are not suitable for control design, novel generalized describing functions were used to integrate performance data with aerothermal models for online simulations [42]. A simpler alternative was to use corrected spool speed and auxiliary coordinates to compute pressure ratio, corrected mass flow and isentropic efficiency [40]. In [72],

the data is extracted from performance maps through commercial software and the component corrected parameter data is encompassed in curve fitted functions. An alternative non-linear compressor map representation is developed through segments of a set of ellipses with moving parameters, the map modelling information is contained through polinomial functions of the rotor speed and an iterative optimization algorithm is used to tune the engine model parameters [63]. These methods usually require accurate performance map information and microturbojet performance maps are usually not available. This lack of information lead to the use of alternatives with a similar approach.

Some alternatives were based on describing the relationship of the engine performance parameters to the engine thermal state, instead of extracting data from the performance maps. For example, efficiency corrections are approximated as polynomial functions of the relative rotor speed, and the mass flow is given as a polynomial function of the pressure ratio [23]. An alternative to the relative isentropic efficiency function is developed to simplify the model computation, the square of the relative shaft speed is used directly with a correction parameter to compute compressor work [5]. These approaches provide an alternative where performance map data is not available.

A different approach for improving the model accuracy is to integrate variable burner efficiency in the combustion chamber due to loss of stochiometry, reduced of atomization or reduced combustion time available [52]. An alternative to compute the combustion temperature with fixed combustion efficiency models, was to use the excess of air factor as an indicator in look-up table empiric information [45]. In an additional research topic, the burner efficiency was analyzed through numerical simulations, where constant burner efficiency models lead to high isentropic efficiency variations to compensate the turbine inlet temperature bias [3]. These effects were observed experimentally in microturbojets, where the burner efficiency was dependent on the engine thermal state with a similar behaviour to the fuel-air ratio [54]. The efficiency variations are an important source of model errors.

General aerial vehicles are submitted to different environmental conditions, the estimation models are required to handle these variations at a wide range of operating conditions. In [59] corrected parameters are incorporated to a modular linear dynamic model to extend the capabilities for the whole operation flight envelop with small variations in the engine thermal state. A non-linear model was developed in [45] for a turbofan engine at varying environmental conditions and operation regimes. The model relies on mass, momentum and energy balances, and empirical information from performance maps. The effects of flight conditions in thrust and component thermodynamic properties were analyzed in numerical simulations for micro turbojets, the main contribution of flight conditions is presented in the form of mass flow and ram drag variations [32]. Modern aircraft operate a wide variety of environments, these effects must be encompassed in the model to accurately estimate its performance parameters.

With the increment of computational power, other means for improving the estimation accuracy were developed. A method based on the Newton Raphson algorithm was implemented to solve a set of non-linear algebraic equations that represent the engine aerothermal characteristics. The model was developed with the aid of block-oriented diagrams according to physical laws contained in each block [71]. The development of non-linear analytic relationships among exhaust gas temperature and shaft speed and fuel flow was achieved through the use of random mutating genetic programming with mean square error as cost function [50]. An advantage is that no information of the component performance maps is required and the structure of the model has a wide range of posibilities. Models based on CFD numerical simulations were developed to estimate thrust and other thermodynamic parameters. The results presented show small percentile error. However, parameters such as turbine inlet temperature and shaft speed were given as model inputs as the simulation could not estimate such complex dynamics [8]. Some recent model-based algorithms include multiobjective adaptation to fit the engine measurements through health parameter optimization [63], including a new performance map generation

method .With these technologies acceptable results were obtained at the expense of computing power. Nevertheless, the time for completing the calculations for some of the models is far to long for real time applications.

3.3 Data-based estimation

The models main objective is to estimate variables which are difficult to measure in flight and to provide information on the engine thermal state [58]. Shaft speed captures dynamic and static engine thermal state with high fidelity and it is the dominant relationship to fuel flow [34], whereas thrust is an important flight variable that can not be measured during flight [76]. Hence, non-linear control oriented models are of particular interest [74]. Shaft speed and thrust dynamics are not captured by conventional thermodynamic models as its physics analysis is complex, thus alternative models have been developed. Black box models are common approaches for these variables [7]. These models are used when few information is available about the system physics. The main problems concerning data-based models are the uncertainty due to signal noise in the measured signal, excitation signal analysis, non-linear effects and defining the model structure.

Sensor noise is a tough problem for model identification, as true dynamics may be hidden in the noise. In 1996 an approach based on averaging the Fourier spectrum coefficients at different time windows was applied. The noise coefficients were smaller than the coefficients coresponding to the model dynamics [26]. In further research coherence functions were implemented for small-signal data tests to reduce the noise effects on the identification procedure [20]. In general, preprocessing before identification is required to reduce the effects of the noise [58].

Earlier methods were based on transfer function coefficients estimation using pseudo random binary sequence (PRBS) inputs [29]. The use of small signal multisine tests allowed the identification of static nonlinearities and improved the engine

identification process in [26]. However, multisine tests do not cover steady state information, require long identification time and provide little information on slow thermal dynamics, while in PRBStests a priori information of the model dynamics is required [58]. Thus, alternative identification signals based on multi-step tests were preferred in [74], as they contain static and dynamic model information.

The zero-pole configuration of the model transfer functions is difficult to determine through a physics-based approach. On the other hand, iterative approaches may not result in the real model structure but in a particular representation for a specific experiment. Earlier least squares identification algorithms lead to unrealistic pole locations when fixed to a certain zero-pole configuration with PRBS signals [29]. Thereafter, different zero-pole configurations were analyzed in terms of simulation error, showing that the low pressure shaft speed dynamics can accurately be modeled by a transfer function with two zeros and three poles [14]. Different nonlinear autoregressive moving average with exogenous input (NARMAX) model structures were proposed, improving the identification results when the input signal to noise ratio is reduced. However, unstable poles were still obtained at some operation points [19]. A systematic approach for developing model structures have not been developed [47], although valuable efforts have been presented.

Turbojet engines posse a highly dominant non-linear gain. NARMAX models were developed to capture the engine nonlinear steady state behaviour, as the look-up tables complicate controller design [27]. In [19] and [55]. It was shown that second order polinomials are sufficient to model static behaviour of the engine. This non-linear static gain is commongly combined with a linear dynamic part in block-oriented models [37, 47]. Alternative models were developed based on equilibrium manifold expansion to provide static accuracy at high thermal states [74]. In [75], a brief evaluation of industrial control-oriented models showed that its accuracy drop below the recently developed technologies for estimating engine dynamics at higher thermal states.

Due to the lack of a clear methodology for developing NARMAX and ARMAX model structures, black box models have been implemented. For example, neural network and genetic programming were implemented in [20] to avoid the structure selection process. In [36], a recurrent neural network models was used to estimate thrust based on pressure and shaft speed measurements. Different neural network structures were analyzed in terms of root mean square error, where the best fitting neural network model was a feedforward neural network with 8 hidden layers [20]. However, neural network models are also dependent on their fundamental structure. Thus, genetic programming was implemented to determine the best suited NARMAX and B-spline models, where B-spline models provide good accuracy for the whole operation regime [55]. Alternatives based on extreme machine learning have been used to develop feedforward neural network structures capable of capturing the fuel-flow to thrust dynamics for a particular operation point [76]. These alternatives provide good accuracy at the cost of model visibility and simplicity.

Black box models present good performance for validating signals similar to the test data. However, these models may lose precision when submitted to untrained conditions. In [49] further experimental evaluation of the models produced by genetic algorithm implementation demonstrated that NARMAX models outperform neural networks for large signal tests. Thus, neural networks were used for the development of an approximate model predictive control. However, for smaller turbojets with higher operation shafts speeds a two layer feedforward neural network with 10 hidden layers outperformed different NARMAX models [60]. Experimental analysis of adaptive neuro fuzzy inference systems (ANFIS) and Hammerstein block-models in microturbines showed that when models are subjected to the untrained data, their accuracy may experience a significant drop; while the errors of block-structured models may diminish by less than 0.3 % when they are subjected to the test data [47].

Recent developments are of particular interest due to the lack of analysis, such as non-conventional conditions or multivariable phenomena. Evaluation of difer-

ent regimes such as start-up conditions are modeled through conventional Cauchi integrals by defining a new acceleration factor, providing good accuracy [44]. Multivariable approaches for control-oriented models were implemented in laboratory facilities with favorable results [34]. To assist model validation more sophisticated technologies based on statistical analysis have been implemented to test the engine models accuracy [73]. These models provide an insight on the new jet engine technology demands.

3.4 Contents review

A mismatch of the fundamental engine structure with the actual engine dynamics can cause model errors, specially with optimized identification of efficiency parameters. After engine modelling, main error sources are stochastic effects, unmodelled dynamics or a mismatch in the non-linear behaviour [26]. A more suitable engine structure can improve the estimation capabilities and operational regimes. This model structure would allow improving application algorithms capabilities, for engine research and industrial applications.

In the present report, a simple and accurate physics-based model calibrated with turbomachinery principles is developed. This model encompasses a fundamental engine structure that improves the estimation capabilities for wider operation conditions. The following contents are included:

- The development of wind tunnel instrumentation for drag and speed measurements, and the engine drag dimensionless coefficient.
- The process of developing the fundamental model structure.
- The structure parameter computation, based in experimental tests.
- The validation of the developed model at different operation regimes and wind speed conditions.

Chapter 4

SR-30 engine

The gas turbine used for the data acquisition was the SR-30, produced by Turbine Technologies Ltd. The gas turbine contains a subsonic inlet, a centrifugal compressor, an annular combustion chamber, a single stage axial flow turbine and a subsonic nozzle. The maximum design rotational speed is 87,000 RPM with a design maximum thrust of 178 N. The start of the engine requires an external source of 689 KPa to spin the rotor up to a speed of 10,000 RPM. Subsequent to this, the fuel injection and ignition begins. The fuel flow is adjusted by a manual lever, which is connected to the valve that controls the flow.

The sensors are located at the exit of the engine stages (Figure 4.1). The test bench contains piezo-resistive pressure transducers and K-type thermocouples at the diffuser, compressor, combustion chamber, turbine and nozzle outlets. Besides the thermodynamic properties, this platform allows to measure thrust, shaft rotational speed and fuel pressure. The thrust sensor is a strain gage load cell. A pressure transducer system measures the fuel pressure and a 2-pole tachometer generator measures the rotational speed of the shaft.

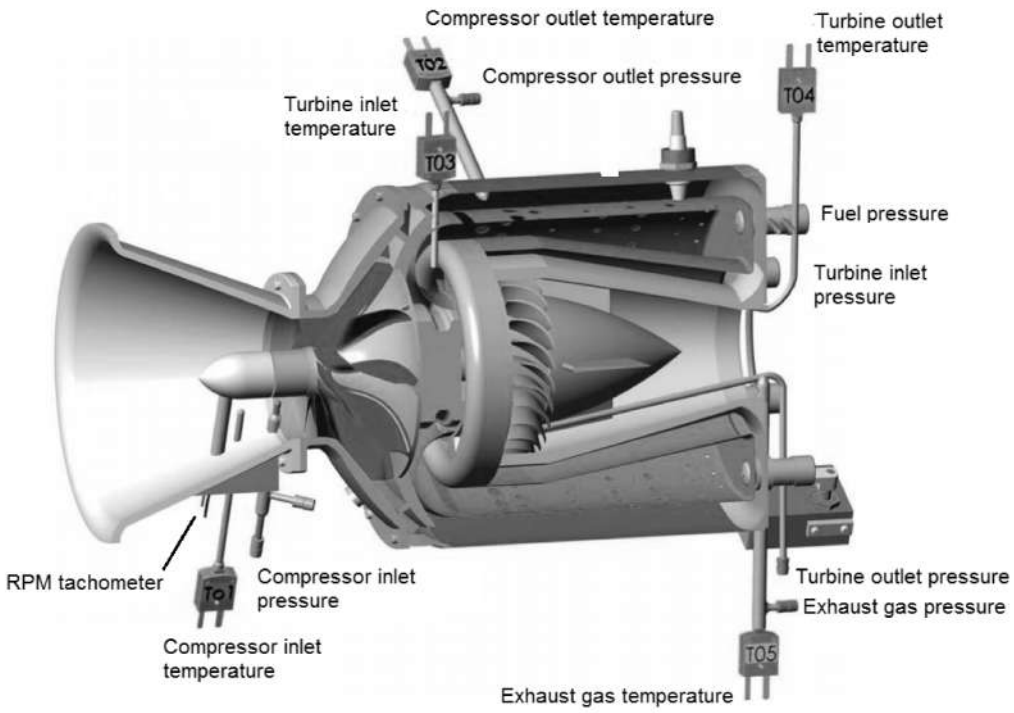

Figure 4.1: Sensor locations.

4.1 Data acquisition system

The platform includes a data acquisition system, based on PCI 4351 card, an A/C board with 24 bit resolution for 16 analogue inputs, a maximum sampling frequency of 60 samples/s for an individual channel and a Virtual Bench Logger data acquisition programme for a live monitoring of the measured variables on a PC. The sampling frequency selected for this experiment was 2.8 Hz to achieve the maximum practical sampling frequency.

Chapter 5

Wind tunnel instrumentation

The ramming wind speed on the engine affects the drag force measurements, therefore it is important to compensate the air resistance effects before the data analysis. This section presents the test bench instrumentation for the aerodynamic drag characterization and its implementation in the SR-30 turbojet. During the tests, wind speeds up to 25 m / s were considered. The drag coefficient and the drag curve versus velocity were obtained. The developed test bench allows accurate measurements of force and air speed in wind tunnel facilities with relatively small perturbations in the flow.

Reducing the drag force in vehicles lead to lower fuel consumption and operation costs, among other benefits. Since the beginning of the aerospace industry, it has been sought to reduce aerodynamic drag. The main factor for reducing costs and pollution is the reduction of aerodynmic drag [15] and allows to achieve greater endurance and operational speed [51].

Figure 5.1 shows an example of the progress on the aerospace industry on the reduction of drag force. The Me 109 fighter lacks of fairing in the section of the landing gear, then a 1972 Cessna with fairing on the landing gear. The Chevron-type fairing is added to reduce the pressure differential between the engine exhaust and the environmental conditions, in order to reduce the noise and the generated

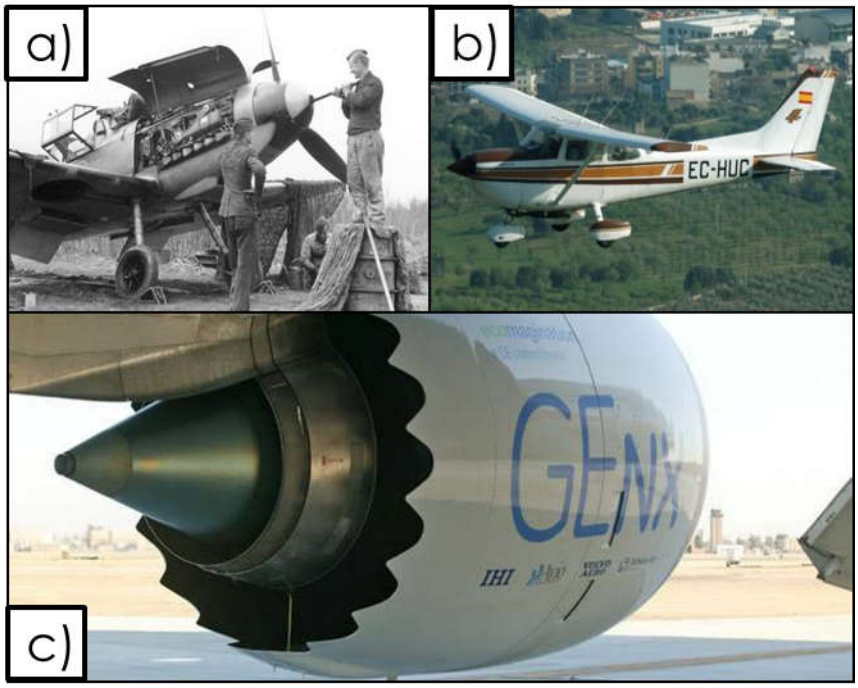

Figure 5.1: Aircraft fairing evolution.

drag.

The ground transport industry has also been interested in the mechanisms of aerodynamic drag reduction. Figure 5.2 shows a conventional trailer (a), the rear fairing aims at decreasing the generation of vortices at the rear of the vehicle (b) and the front fairing to reduce the ram drag (c). Some of the studied ground vehicle drag reduction mechanisms are:

- The use of vortex generators in civilian vehicles to reduce drag at low speeds [33].
- The effects of devices designed for heavy vehicles, such as lower, front and rear fairing [56].
- Modifications that allow a reduction of up to 26 % less drag force, which require few structural changes [21].
- Simple devices that reduce up to 10 % less drag force in heavy vehicles [70].

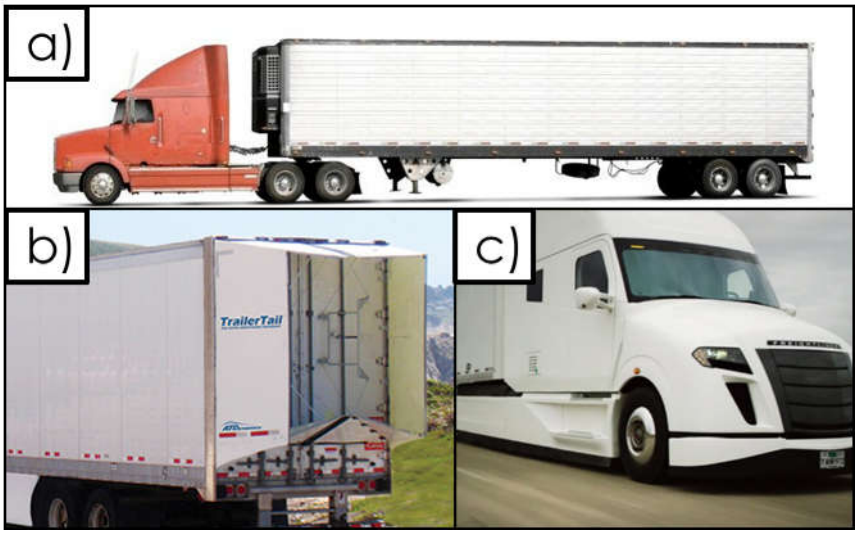

Figure 5.2: Heavy truck fairing evolution

5.1 Background of wind speed measurements

Figure 5.3 shows some of the most common methods for measuring speed in wind tunnels. Currently, flow velocity measurements are made using different instruments, such as [10]:

- Pitot tube, shown in Figure 5.3 a). Estimate the flow velocity considering the difference between the static and total pressure. It disturbs the flow since it requires a support, and only makes punctual measurements of speed.
- A hot wire anemometer is shown in Figure 5.3 b). These devises provide precision in fast changes of speed and disturb the flow in a lesser degree. This equipment may be relatively more expensive devices and require constant calibration.
- Particle image velocimetry is represented by Figure 5.3 c). It is a non-invasive mode that illuminates the flow contaminated with particles, the refraction is absorbed and used to calculate the speed. It is problematic in closed configurations, since the particles accumulate inside the tunnel. The speed measure-

ments correspond to a cross section of the wind tunnel.

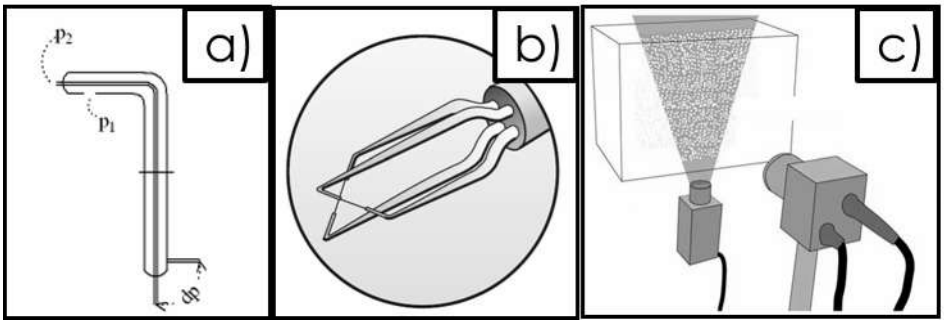

Figure 5.3: Common wind speed measurement devices.

5.2 Background of wind tunnel force measurements

The magnitud of the components of the aerodynamic forces is obtained through direct measurement, pressure distributions on the model surface, the effects that the model on the flow or the movement of the model under the applied aerodynamic loads [10]. These methods are presented in the Figure 5.4: Section a) shows the pressure distribution instrumentation scheme for the surface of an aerofoil. Section b) shows the effects of an airfoil on the wind flow. Finally, Section c) shows a platform to study the pitch dynamics of an aircraft.

The scales can be placed internally or externally to the wind tunnel. Generally, internal mechanisms are placed when displacement is required in the model. The scales can become very complex depending on the degrees of freedom to measure.

A common problem in the aerodynamic scales are hysteresis loops dependent on the wind speed. These loops present a greater amplitude when approaching to 0, as shown in Figure 5.5.

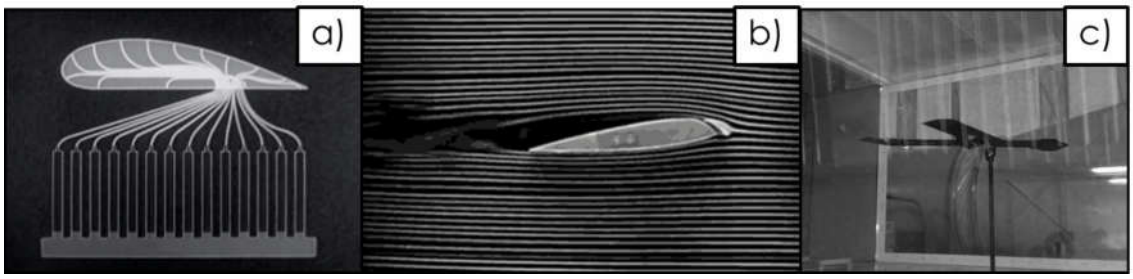

Figure 5.4: Aerodynamic force measurement devices.

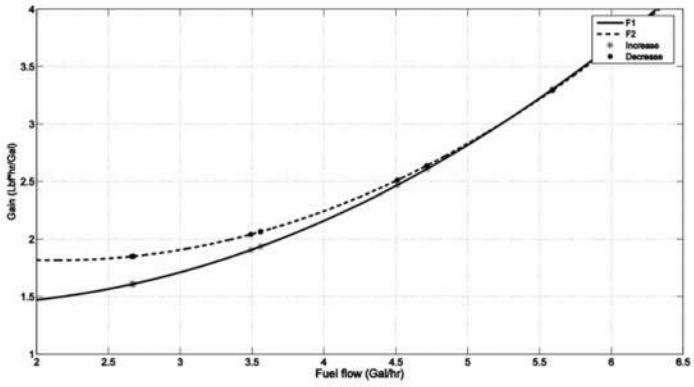

Figure 5.5: Hysteresis loops in aerodynamic scales [62].

5.3 Characterization of flow transition zone

Flow visualization techniques were implemented to determine the transition conditions of the wind tunnel previous to the test bench design, Figure 5.6.

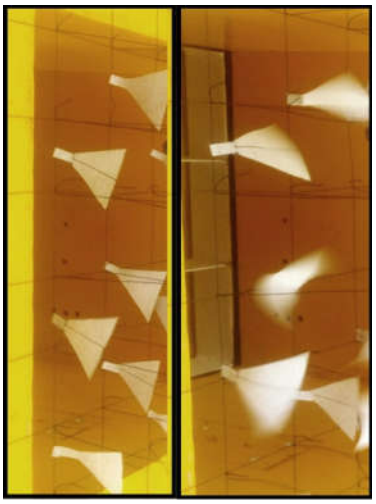

Figure 5.6: Laminar flow (left) and turbulent flow (right).

Visulalization techniques were implemented to observe:

- Turbulence: through erratic and abrupt movements in the tufts.
- Rotational fields: characterized by the twisting of short fins.

The laminar-turbulent transition ocurred at a Reynolds number of 229,000 and at a wind speed of 12.38 m / s. This is similar to the conditions reported in similar conditions [69]. These types of qualitative techniques have been widely used in the aeronautical sector [17], [57].

5.4 Test bench development

To measure the wind speed by means of a non-invasive method, the algorithm was based on static pressure taps in known cross-sectional areas. The total pressure in

each tap is defined according to the Bernoulli principle by:

$$P_T = P_S + P_D \tag{5.1}$$

The dynamic pressure is defined as:

$$P_D = \frac{1}{1}\rho V^2 \tag{5.2}$$

The mass flow is conserved at every section of the wind tunnel, as there are no mass exchange sections.

$$\frac{dm}{dt} = \rho_\alpha V_\alpha A_\alpha - \rho_\beta V_\beta A_\beta = 0 \tag{5.3}$$

Therefore, a static pressure differential is defined in the form of::

$$\Delta P_S = P_{S\alpha} - P_{S\beta} = P_{D\beta} - P_{D\alpha} \tag{5.4}$$

The wind speed change is now a function of the change in the static pressure:

$$P_{S\alpha} - P_{S\beta} = \frac{1}{2}\rho(V_\beta^2 - V_\alpha^2) \tag{5.5}$$

Thus, the relationship between the static pressure differential and the wind speed is:

$$V_\beta = \sqrt{\frac{2(\Delta P_S)}{\rho}\left(1 - \left(\frac{A_\beta}{A_\alpha}\right)^2\right)^{-1}} \tag{5.6}$$

The speed estimation was initially calibrated by means of a hot wire anemometer.

The force was measured by a scale, as presented in figure 5.7. Based on a balance of moments, at one end of a straight elbow the model was placed inside the wind tunnel and at the opposite end a load cell was placed. The preload (F_l) has the function of calibrating and improving the quality of the measurements. The drag force (D) is:

$$D = F_l - F_M \tag{5.7}$$

F_M is the load cell measured force.

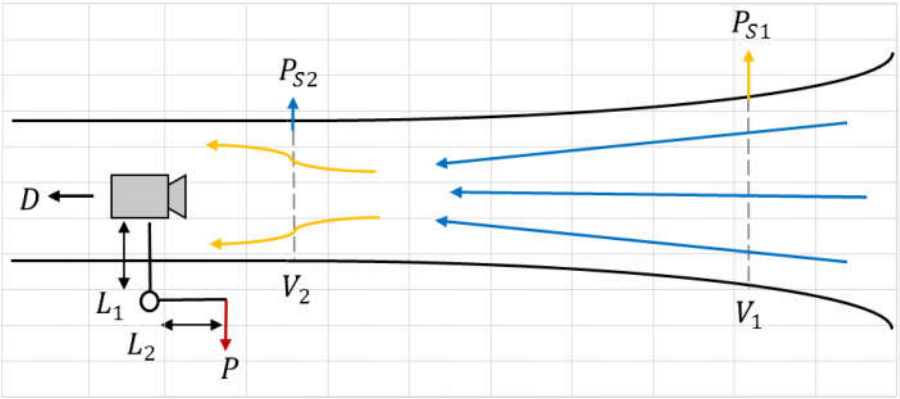

Figure 5.7: Diagram of the test bench.

Therefore, the average drag coefficient for n tests is defined as:

$$C_D = \frac{2}{\rho S m} \sum_{i=1}^{u} \left(\frac{2(\Delta P_s)}{\rho} \left(1 - \left(\frac{A_2}{A_1} \right)^2 \right)^{-1} \right) \tag{5.8}$$

5.5 SIGNAL PROCESSING

The drag force generated was measured for a wind speed range from 0 to 25 m / s with a preload of 15.84N. Figure 5.8 presents the wind speed signal self-correlation, calculated to determine the fundamental frequency due to the high level of noise

and uncertainty. This figure shows that the implemented sensors do not detect any relevant oscillatory dynamics. Thus, a low pass filter was designed to eliminate high frequency noise, the filter effect is observed in Figure 5.8.

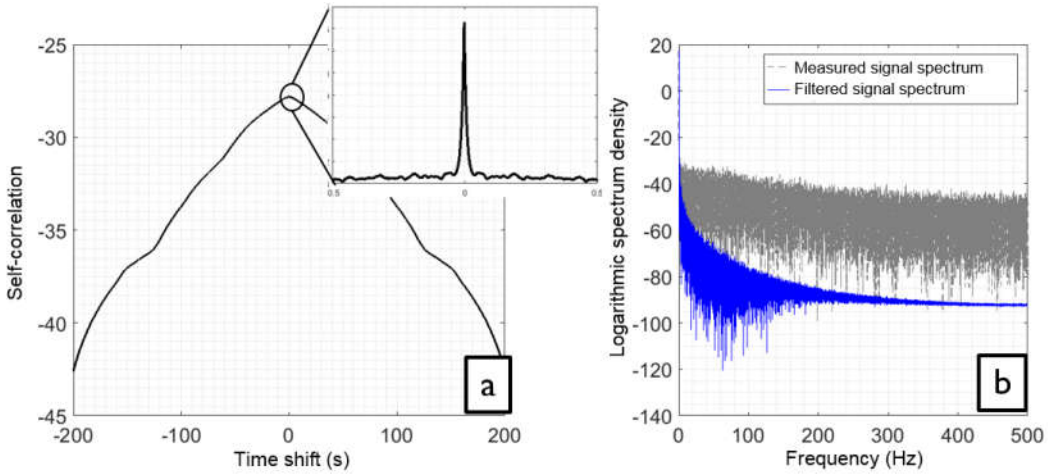

Figure 5.8: Wind speed measurements frequency domain analysis.

Figure 5.9 shows the velocity measurements for a calibration test performed with the turbojet engine. The filtered measurements show a small band of uncertainty and keep a steady value close to that of the hot wire anemometer. This shows that:

- The noise and uncertainty increase with the flow velocity.
- The objective of reducing the noise level in the signal was achieved.
- A more manageable wind speed signal was obtained.

Figure 5.10 shows the spectral density of the measured drag force. Due to the presence of high frequency noise a low pass filter with a cutoff frequency of 0.033 Hz was implemented. Only the steady state of the measurements was retained.

The measurements during the characterization test performed of the SR-30 engine are shown in Figure 5.11. The filter reduced the noise and allowed to visualize the average value of the speed. Tests were performed with ascending and descending

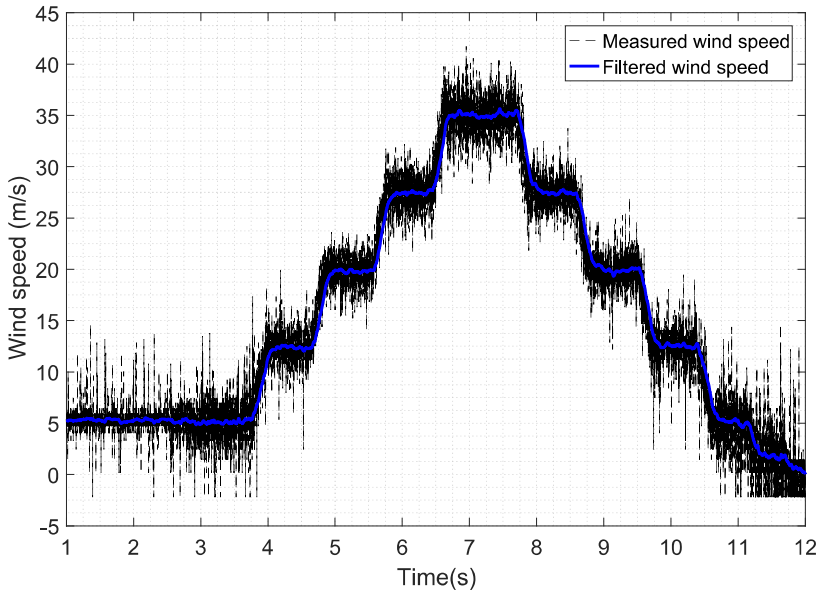

Figure 5.9: Measurements of wind speed before and after low pass filtering.

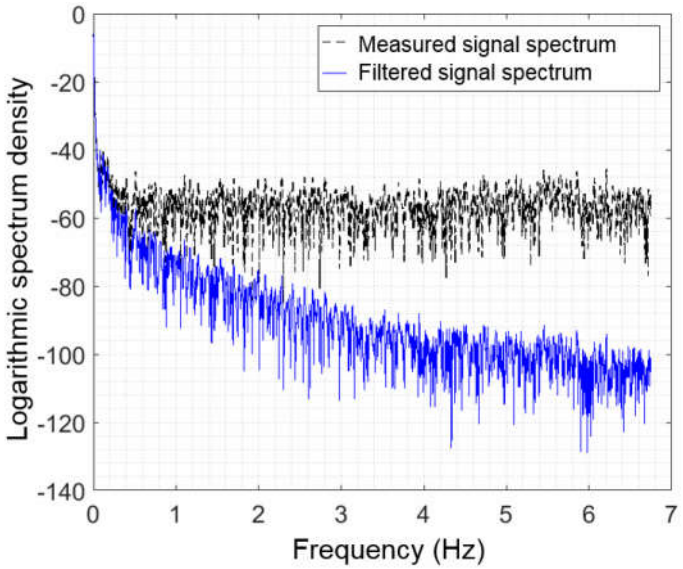

Figure 5.10: Frequency analysis of the drag force measurement signal.

velocities to evaluate the effectiveness of the test bench in preventing hysteresis loops. The turbulent flow presented from 11.9 m / s, this low speed is due to the configuration as an impact wind tunnel.

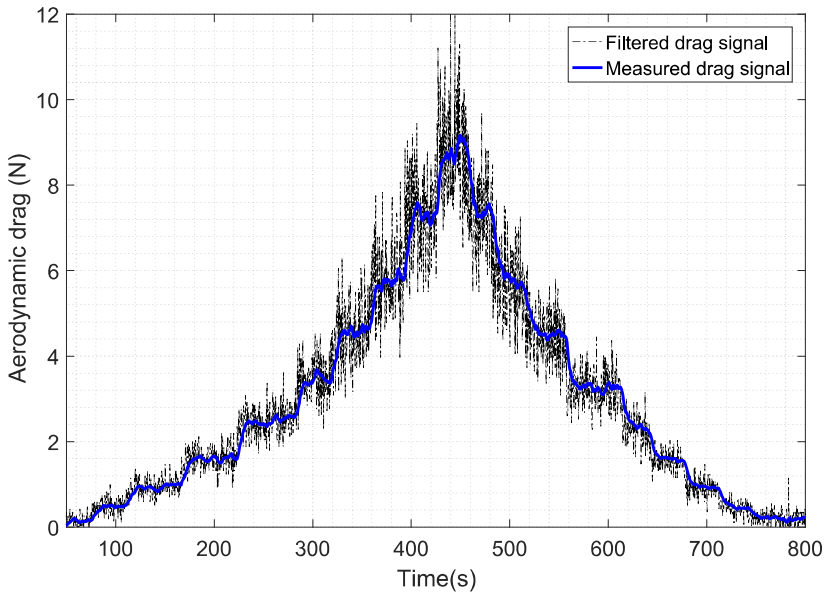

Figure 5.11: Drag force measurements before and after the low pass filtering.

5.6 Drag force characterization

The drag force measured is presented in Figure 5.12. The measured drag force approaches to a quadratic function with the speed (as expected), the computed dimensionless drag coefficient is 0.139. The drag coefficient does not vary with the operating conditions.

The developed instrumentation allows cost-effective alternatives to wind tunnel measurements. Accurate wind speed measurement can be obtained without disturbing the airflow with low-cost platforms. The speed estimation presented good results for a wide range of operating conditions. Uncertainty increases after the identified laminar-turbulent flow transition zone. The implementation of signal processing techniques allows obtaining a precise value of the measurements, despite working in

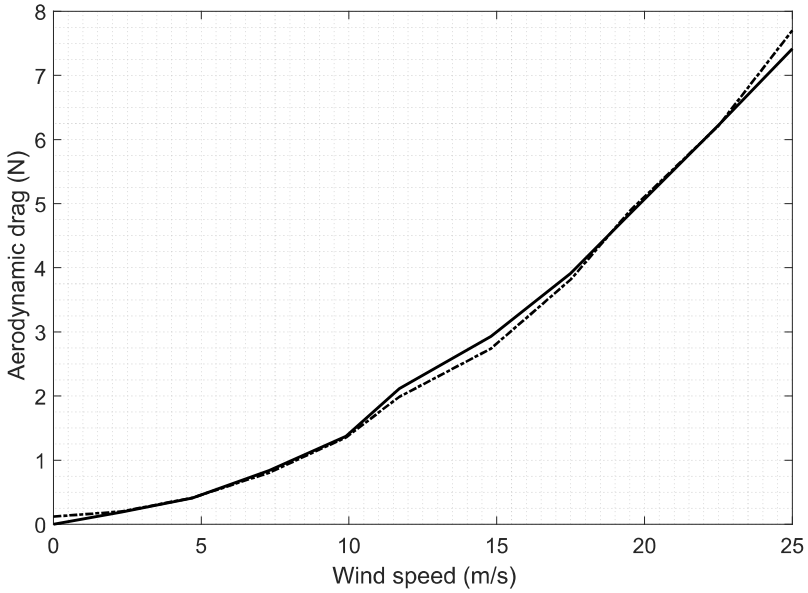

Figure 5.12: Drag force versus wind speed.

conditions of turbulence, noise and uncertainty.

In the experiments, the drag coefficient appears to be independent of the flow velocity. In particular during descending or ascending of the wind speed. The calculated drag coefficient is similar to values computed in other studies [61]. This shows that, the developed test bench allows to characterize the aerodynamic drag force in wind tunnel models. Moreover, hysteresis loops were not found when raising or lowering the speed [67]. This platform also allows to evaluate the effects of the fairing or structural modifications in models subject to a wind flow, such as aircraft and land vehicles.

Chapter 6

Turbojet physics modelling

The micro turbojet used for the tests is presented in the Figure 6.1. The analysis of the micro-turbojet is simplified analysing independently each one of the engine components. A control volume is defined for each engine component and the interaction among the variables is defined through sets of state equations.

1. Inlet
2. Compressor
3. Combustion Chamber
4. Turbine
5. Nozzle

6.1 Nozzle and inlet analysis

There is no shaft work and the heat transfer is minimal, as high flow speed prevents the fluid from being in contact with the engine surface long enough to transfer an appreciable amount of heat [31]. Therefore, the jet engine behaviour is independent of the heat transfer [9].

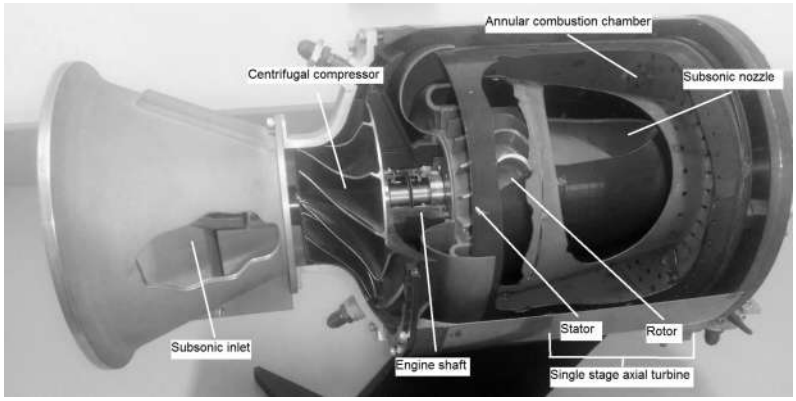

Figure 6.1: Engine cutaway view.

The turbojet nozzle increases the exit velocity as it expands. In a subsonic accelerating nozzle the cross-sectional area decreases while in a supersonic accelerating nozzle it first decreases until the fluid reaches the speed of sound and then increases to allow the fluid to overcome this velocity [18]. The first law of thermodynamics in this section is described as:

$$0 = \dot{m}(h + \frac{V^2}{2})_e - \dot{m}(h + \frac{V^2}{2})_i \tag{6.1}$$

The compressor inlet conditions are available through sensor measurements. For simplicity, the nozzle pressure and temperature ratios are assumed as constant, due to design conditions, instead of a deeper modelling of the expansion and flow acceleration mechanisms.

6.2 Turbine and compressor

The heat transfer is negligible due to the flow speed, however, the shaft dynamics are an important parameter in this section. In turbines the air impacts the blades generating work, the fluid expands and the temperature decreases. In compressors the process is opposite, where the compressor applies work by means of the blades to increase the pressure in the fluid. In a turbojet engine these components are attached

by a rigid shaft, thus the work substracted by the turbine is the work excerted by the compressor [31]. According to conventional mass and energy conservation, the equation for stationary flow becomes:

$$-\dot{W}_x = \dot{m}_x(h + \frac{V^2}{2})_e - \dot{m}_x(h + \frac{V^2}{2})_i \tag{6.2}$$

Note that the total stagnation temperature is given by:

$$T_T = \frac{h}{C_p} + \frac{V^2}{2C_p} \tag{6.3}$$

However, the non-linear static and dynamic behaviour of the turbojet is dependent on the thermal state. Therefore, an alternative to compute the shaft work based on Eulers turbomachinery equations [46] is presented:

$$\dot{W}_x = \dot{m}_x N(r_e V_e - r_i V_i) \tag{6.4}$$

Where the tip speed is described as a function of the rotational speed and component radius:

$$V_x = N r_x \tag{6.5}$$

6.2.1 Compressor analysis

Figure 6.2 presents a velocity diagram of the SR-30 centrifugal flow compressor, thus the inlet radius is smaller than the exit radius.

$$r_i \gg r_e \tag{6.6}$$

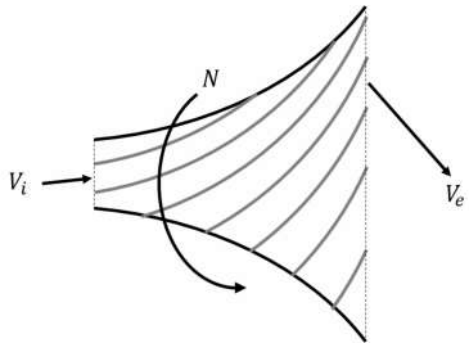

Figure 6.2: Compressor diagram

Thus, the compressor total work can be described as a function of the rotational shaft speed:

$$\dot{W}_c = \dot{m}_0 N^2 r_e^2 \tag{6.7}$$

6.2.2 Turbine analysis

The turbine is a single stage axial turbine. The inlet and exit radius are similar and the exit speed is much greater than the input speed, due to the high rotational speeds in which microturbojets work.

$$r_i \approx r_e \tag{6.8}$$

$$\begin{aligned} V_e &= Vi + Nr_e \\ V_e &\approx Nr_e \end{aligned} \tag{6.9}$$

Thus, the turbine work equation becomes:

$$\dot{W}_T = \dot{m}_T N^2 r_e^2 \tag{6.10}$$

6.2.3 Integration in to the thermodynamic model

For both, the turbine and the compressor, Euler turbo machinery equations can be used to compute the shaft work. Then, the shaft work is used to compute the exit total temperature:

$$T_{Te} = T_{Ti} \pm \eta_x \frac{r_e^2}{C_{px}} N^2 \tag{6.11}$$

Where the sign depends on the work direction. Positive if it is added to the fluid and negative if it is subtracted from the fluid.

Thereby, the pressure ratio for the compressor is computed with the temperature ratio and correction with the poly-tropic efficiency, in the form of:

$$\pi_c = \tau_c^{\frac{e_c \gamma_c}{\gamma_c - 1}} \tag{6.12}$$

In a similar form, the turbine pressure ratio is computed as:

$$\pi_t = \tau_t^{\frac{\gamma_t}{e_t(\gamma_t - 1)}} \tag{6.13}$$

The pressures computation is based on isentropic relationships.

6.3 Combustion chamber

The fuel enters the chamber and mixes with the reactants. The fuel is burned and heat is produced, the combustion steady-state equation describes a fundamental relationship among the chemical energy added in the form of fuel and the change in the products temperature [66]. Thus, a change in the chemical energy stored in a

sustance due to its chemical composition (entalpy of formation) produces a change in the products tempeature (sensitive enthalpy) [38]:

$$(h_f^o + \Delta h^o)_{cr} = (h_f^o + \Delta h^o)_p \tag{6.14}$$

An alternative combustion equation for stationary flow is described using temperatures instead of sensitive enthalpies:

$$(h_f^o + C_{Pcr}(T_{cr}))_{cr} = (h_f^o + C_{Pp}(T_P))_p \tag{6.15}$$

The heat released by the combustion process is used to increase the temperature of the products, the amount of heat is dependent on the amount of mass and the difference among the reactive and product formation enthalpy[66]. The enthalpy of combustion is the heat released when burning a certain fuel.

$$h_c^o = h_{fcr}^o - h_{fP}^o = C_{Pcr}(T_{cr}) - C_{Pp}(T_p) \tag{6.16}$$

The lower calorific value is used instead of the combustion enthalpy to simplify the computations, as it is a mass-dependent parameter instead of a molar-dependent parameter [66]:

$$PCI = \frac{|h_c^o|}{M_m} \tag{6.17}$$

Thus, a more convenient approach is to analyze the combustion process as a function of air mass, temperatures and fuel mass flow [46]. An efficiency factor is added to integrate incomplete combustion, loss of stochiometry or fuel mixture variations during operation.

$$\eta_b \dot{m}_f PCI = \dot{m}_T C_{Pt} T_{T3} - \dot{m}_0 C_{Pc} T_{T2} \tag{6.18}$$

Note that the mass flow after the combustion chamber is the sum of the air mass flow and the fuel mass flow:

$$\dot{m}_T = \dot{m}_0 + \dot{m}_f \tag{6.19}$$

Althouth the combustion efficiency is held constant in conventional thermodynamic models, previous research observed that the burner efficiency is not constant during the different engine thermal states [3] [54]. The major contribution for this component is to model the burner efficiency variations through curve fitting at different engine thermal states.

6.3.1 Least squares algorithm

The burner efficiency is fit through least squares estimation with a second order polynomial. The regression algorithm calculates the most fitted parameters to minimize the quadratic error of the burner efficiency at several operation points. A compact form of the algebraic expression is:

$$y(j) = X(j)\theta + e(j) \tag{6.20}$$

With the cost function denoted as:

$$J = (y(j) - X(j)\theta)^2 = e(j)^2 \tag{6.21}$$

Where θ denotes an unknown parameter vector, which consists of the coefficients of a polynomial function, expressed in the form of:

$$\begin{aligned} y_1 &= b_0 + b_1 o_1^1 ... b_k o_1^k \\ y_2 &= b_0 + b_1 o_2^1 ... b_k o_2^k \\ &\vdots \\ y_j &= b_0 + b_1 o_j^1 ... b_k o_j^k \end{aligned} \tag{6.22}$$

Which is a polynomial of dimension k computed with j data samples, also represented in a matrix form:

$$\begin{aligned} \theta &= [b_0 ... b_k]' \\ X &= \begin{bmatrix} o_1^0 & ... & o_1^k \\ \vdots & \ddots & \vdots \\ o_j^0 & ... & o_j^k \end{bmatrix} \\ Y &= [y_1 ... y_j]' \end{aligned} \tag{6.23}$$

The minimal value of the cost function is found by zeroing the derivative of the equation 6.20 as a function of θ. Accordingly, the best suited parameter vector for the given conditions is calculated according to [30]:

$$\theta = [X^T X]^{-1} X^T Y \tag{6.24}$$

This estimation method will be used in the next chapter to compute a burner efficiency to shaft speed polynomial function.

6.4 Performance parameters

Several parameters determine the performance of the motor, such as thrust, specific fuel consumption and thermal efficiency. As thrust is an important parameter that can not be measured during flight, it will be the main performance parameter analyzed in this document. The generated thrust F of a jet engine is given by the

change in the linear momentum at the input and output of the motor [48].

$$F = (\dot{m}_o + \dot{m}_f)V_e - \dot{m}_o V_o + (P_e - P_o)A_e \tag{6.25}$$

It is desirable to expand the gases to the ambient pressure to increase the thrust, thus a common assumption is to consider that the inlet pressure and the exit pressure are approximate. The thrust equation equation is rewritten as:

$$F = (\dot{m}_o + \dot{m}_f)V_e - \dot{m}_o V_o \tag{6.26}$$

The exit speed computation requires solving a set of non-linear equations and include some parameter assumptions. These non-linear equations involve the compressible flow equations and the environmental speed of sound to compute the exhaust gas; with the assumption that the ratio of exit pressure to ambient pressure is constant during operation [46]. An alternative process to compute thrust is proposed in this document, based on mass conservation equivalences. Note that:

$$V_x = \frac{\dot{m}_x}{A_x \rho_x} \tag{6.27}$$

Thus, the thrust equation can be rewritten in terms of mass flow, density and cross-sectional areas:

$$F = \frac{\dot{m}_e^2}{A_e \rho_e} - \dot{m}_o V_o \tag{6.28}$$

The previous equation is dependent of the free-stream speed and aircraft operate at different wind speeds. The second term corresponds to the ram drag. That is the aircraft is displacing at a relative speed with respect to the wind [32]. Thus, a thrust equation developed to handle wind speed variations is presented in this document as:

$$F = \frac{\dot{m}_e^2}{A_e \rho_e} - \dot{m}_0 V_\infty \tag{6.29}$$

Where the first term is the output gas linear momentum, the second term involves the ramming air linear momentum to the engine.

6.5 BLOCK-DIAGRAM MODEL

The micro turbojet steady state behaviour is represented through a block diagram model, which comprehends the component equations and the relationships among the thermodynamic variables. The Figure 6.3 presents the non-linear block diagram model.

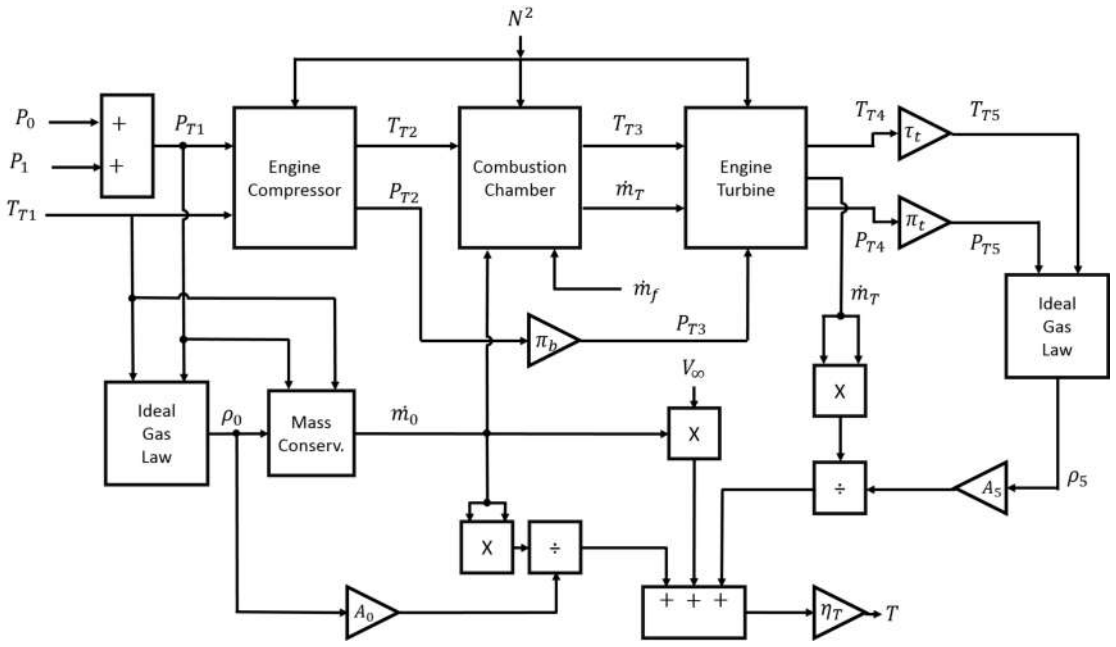

Figure 6.3: Block diagram of the micro turbojet.

The model inputs are the external operation conditions (P_0 and V_∞), the engine inlet conditions (P_{T1} and T_{T1}) and the thermal state indicators (m_f and N), thus no extra sensors are required for on-line implementation. Although the model is developed to estimate thrust, the thermodynamic variables can be monitored, these

states are: compressor, combustion chamber, turbine and nozzle output temperatures and pressures. Thus, additional variables are added to the validation tests, these variables are important health indicators used widely for jet engine monitoring: compressor exit pressure and inlet turbine temperature. The compressor exit properties are used as indicators for surge margins [72], which constrain the engine safe operation due to physical limits [43]. The turbine inlet temperature is used as a thermal state indicator related to thermal efficiency and physical limitations due to the temperature limits [34].

The component pressure ratios (π), temperature ratios (τ) and model efficiencies (η) are represented in the form of static gains. The equation in the engine compressor, combustion chamber and engine turbine blocks are presented in the Table 6.1.

Table 6.1: Equations in the block diagram model.

Model block	Contained equations
Engine compressor	Equations 6.12 and 6.13
Combustion chamber	Equations 6.18 and 6.19
Engine turbine	Equations 6.11 and 6.13

The remaining model blocks are:

- The ideal gas law blocks, used to compute the flow density by solving the gas state equation:

$$\rho_x = \frac{P_{Tx}}{RT_{Tx}} \tag{6.30}$$

- The mass conservation block, used to compute the mass flow:

$$\dot{m}_0 = A_0 \rho_0 V_0 \tag{6.31}$$

Where the speed is computed from pressure differentials:

$$V_0 = \sqrt{\frac{2(P_{T1} - P_0)}{\rho_0}} \tag{6.32}$$

6.5.1 Jet engine instrumentation and model inputs

The model is designed to work with the conventional turbojet on-board instrumentation [41] [6] [53], presented in the Table 6.2.

Table 6.2: Common turbojet on-board gas-path instrumentation sets.

Symbol	Variable	Model input
T_0	Ambient temperature	Yes
P_0	Ambient pressure	Yes
P_{T1}	Compressor inlet total pressure	Yes
N	Shaft speed	Yes
m_f	Fuel flow rate	Yes
T_{T2}	Compressor exit total temperature	No
P_{T2}	Compressor exit total pressure	No
T_{T4}	Turbine exit total temperature	No
P_{T4}	Turbine exit total pressure	No
T_{T5}	Exhaust gas total temperature	No
P_{T5}	Exhaust gas total pressure	No

The model requires fewer sensors than the common on-board instrumentation during flight. This makes hardware redundance feasible, which leads to improvement posibilities for fault detection systems [16] and allows to evaluate the engine variables to a baseline estimation.

6.6 Conventional thermodynamic model

An aditional framework for comparison is developed based on conventional performance theory [46]. The model uses dimensionless parameters computed in reference conditions and then uses thermodynamic laws to extrapolate the thermodynamic variables to the different engine operation conditions. The model inputs are the environmental conditions, the flight conditions and the turbine inlet temperature. This conventional model is used to evaluate the accuracy of the developed engine model to conventional performance algorithms. The first steps compute the inlet conditions in the form of dimensionless ratios, from the input conditions and engine reference values:

$$a_0 = \sqrt{\gamma_i R_i T_i} \tag{6.33}$$

$$V_0 = a_0 M_0 \tag{6.34}$$

$$\tau_r = 1 + \frac{\gamma_i - 1}{2} M_0^2 \tag{6.35}$$

$$\pi_r = \tau_r^{\frac{\gamma_c}{\gamma_c - 1}} \tag{6.36}$$

$$\eta_r = 1 - 0.075(M_0 - 1)^{\frac{\gamma_c}{\gamma_c - 1}} \tag{6.37}$$

$$\pi_d = \pi_{dmax} \eta_r \tag{6.38}$$

Thereafter, the temperature ratio is computed from reference the thermal state variable, which is the turbine inlet temperature, and the environmental temperature.

$$\tau_\lambda = \frac{C_{Pt} T_{T3}}{C_{Pc} T_0} \tag{6.39}$$

Some thermodynamic variables and reference ratios are computed for further use:

$$T_{T1} = T_0 \tau_r \tag{6.40}$$

$$\tau_{rR} = 1 + \frac{\gamma_i - 1}{2} M_{0R}^2 \tag{6.41}$$

$$\pi_{rR} = \tau_{rR}^{\frac{\gamma_c}{\gamma_c - 1}} \tag{6.42}$$

The compressor temperature and pressure ratios are computed using reference ratios, the computed compressor inlet temperature and the input thermal state. This process assumes that the temperature ratio is linear to the change in the engine thermal state:

$$\tau_c = 1 + (\tau_{cR} - 1) \frac{T_{T3}/T_{T1}}{(T_{T3}/T_{T1})_R} \tag{6.43}$$

$$\pi_c = [1 + \eta_c(\tau_c + 1)]^{\frac{\gamma_c}{\gamma_c - 1}} \tag{6.44}$$

Thereafter, the fuel to air ratio is computed with an energy balance in the combustor, where the combustion temperature is assumed to be constant for the operation regimes:

$$f = \frac{\tau_\lambda - \tau_r \tau_c}{PCI \eta_B / (C_{Pc} T_0 - \tau_\lambda)}) \tag{6.45}$$

The pressure ratio of the engine is computed with the individual component pressure ratios. The ratios of the exhaust and environmental, turbine and nozzle pressures are assumed to be independent of the engine thermal state and operation conditions:

$$\frac{P_{T5}}{P_5} = \frac{P_0}{P_5}\pi_r\pi_d\pi_c\pi_b\pi_{tR}\pi_{nR} \tag{6.46}$$

The exit Mach number is computed using the computed pressure ratios:

$$M_5 = \sqrt{\frac{2}{\gamma_t - 1}\left[\left(\frac{P_{T5}}{P_5}\right)^{\frac{\gamma_t - 1}{\gamma_t}} - 1\right]} \tag{6.47}$$

The sensitive pressure ratio is computed through the total pressure changes in the engine and the total pressure ratio of the exhaust conditions.

$$\frac{T_5}{T_0} = \frac{\tau_\lambda \tau_t}{(P_{T5}/P_5)^{\frac{\gamma_t - 1}{\gamma_t}}}\frac{C_{Pc}}{C_{Pt}} \tag{6.48}$$

The exhaus gas speed to environmental sound speed is computed as an auxiliary factor:

$$\frac{V_5}{a_0} = M_9\sqrt{\frac{\gamma_t R_t T_5}{\gamma_c R_c T_0}} \tag{6.49}$$

Thus, the specific thrust is computed through:

$$\frac{T}{\dot{m}_0} = a_0\left[(1+f)\frac{V_5}{a_0} - M_0 + (1+f)\frac{R_t}{R_c}\frac{T_5/T_0}{V_5/a_0}\frac{1 - P_0/P_5}{\gamma_c}\right] \tag{6.50}$$

The mass flow is corrected for different operation regimes, dependent on the engine thermal state and operation conditions:

$$\dot{m}_0 = \dot{m}_{0R} \frac{P_0 \pi_r \pi_d \pi_c}{(P_0 \pi_r \pi_d \pi_c)_R} \sqrt{\frac{T_{T4R}}{T_{T4}}} \tag{6.51}$$

Finally, the turbojet thrust is computed with the mass flow corrections and specific thrust:

$$T = \dot{m}_0 \frac{T}{\dot{m}_0} \tag{6.52}$$

Some considerations are that the compressor characteristics are dependent on the turbine work, thus the temperature estimation errors are accumulated and the model thermal state is based on turbine inlet information, which is not as reliable as the shaft speed measurements [34].

Chapter 7

Identification experimental tests

The experiments consisted in multi-step fuel flow inputs, which offer wider information of the process steady state and dynamic components [74]. The total temperatures and pressures were measured at the exit of each component, the measurements correspond to the Figures 7.1 and 7.2. A superficial analysis of the temperature measurements allows observing that the temperature dynamics depend on the turbojet thermal state; at lower thermal states the temperature presents a slight overshoot, while at higher thermal states no overshoot is observable.

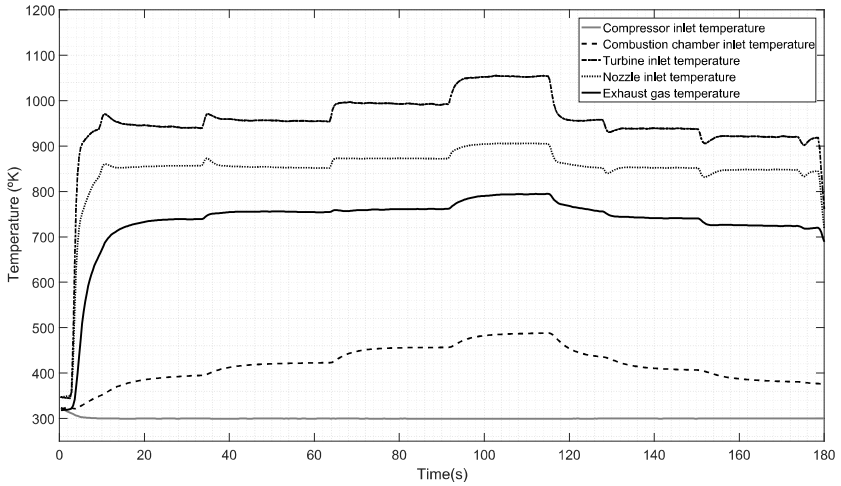

Figure 7.1: Identification experiments temperature measurements.

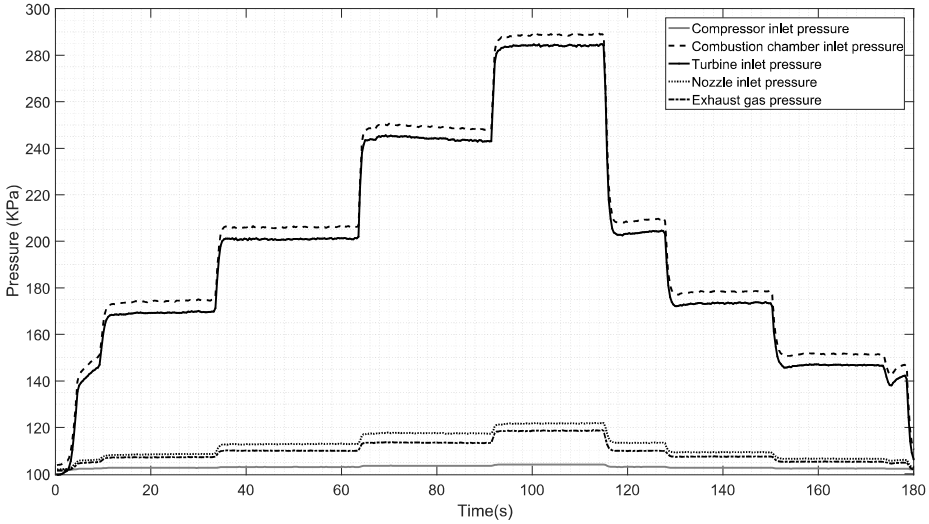

Figure 7.2: Identification experiments pressure measurements.

Additionally, the thrust, shaft speed and the fuel flow were also recorded through the available instrumentation. These variables are presented in the form of normalized variables in the Figure 7.3. This Figure demonstrates a clear non-linear static relationship of thrust and shaft speed to fuel mass flow, as the static gain is different dependent on the thermal state.

The steady state values of the operation condition are obtained by averaging the values in a window time of 20s after the fuel flow change. A total of 7 engine steady state conditions are analyzed. The shaft speed for the developed model input is converted to $rads/s$.

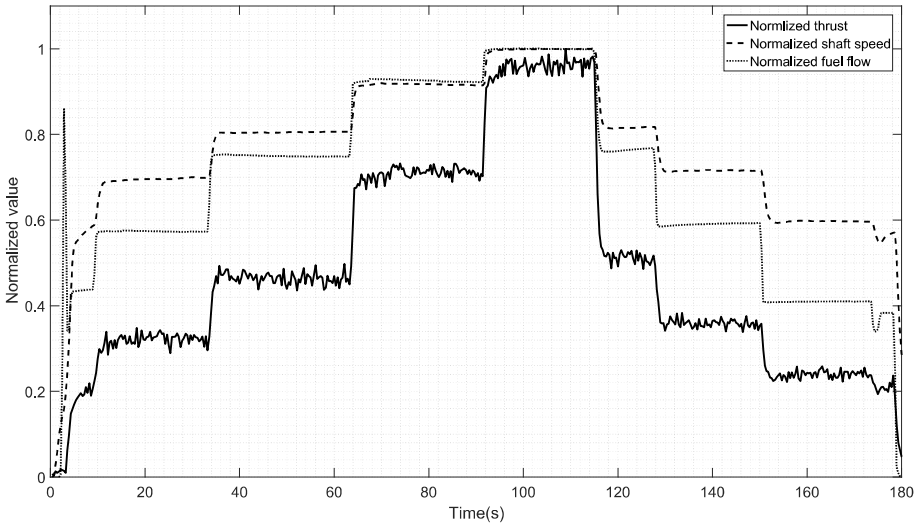

Figure 7.3: Thrust, shaft speed and fuel flow measurements for the identification test.

Chapter 8

Turbojet model data calibration

There is a need for clear procedures to calibrate turbojet models to fit actual engine data [9]. Therefore, a simple procedure to calibrate engine parameters is presented as follows. The turbojet component equations acquire the form of a simple health management algorithm, where the engine efficiency parameters are computed for the algorithm identification process. The engine thermodynamic measurements are used to compute the efficiencies at each operation condition. The tests were performed by locating the SR-30 engine in an impact wind-tunnel to subject the engine to different wind speeds. Figure 8.1 presents the test set-up.

Figure 8.1: SR-30 with wind tunnel set-up.

The test wind speed was registered through the wind tunnel instrumentation

in the Chapter 5.

8.1 Compressor and turbine efficiencies

In order to model the compressor and turbine components a thermal efficiency is required to relate shaft speed to work and change in temperatures to change in pressures. The thermal efficiency is:

$$\eta_x = |\frac{C_{Px}(T_{Te} - T_{Ti})}{N^2 r_e^2}| \tag{8.1}$$

The model considers a linear relationship between temperature change to shaft speed, Figure 8.2 presents the experiments performed to demonstrate this relationship.

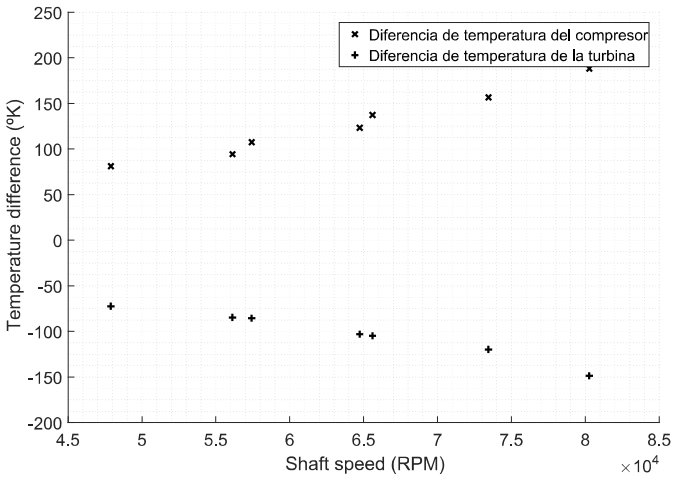

Figure 8.2: Temperature difference to shaft speed.

The polytropic efficiency is used to calibrate the isentropic relationship of the compressor and the turbine behaviour. These efficiencies are computed as [46]:

- Compressor polytropic efficiency:

$$e_c = \frac{\gamma - 1}{\gamma} \frac{ln(\pi_c)}{ln(\tau_c)} \tag{8.2}$$

- Turbine polytropic efficiency:

$$e_t = \frac{\gamma}{\gamma - 1} \frac{ln(\tau_t)}{ln(\pi_t)} \tag{8.3}$$

8.2 COMBUSTION CHAMBER

As mentioned before, the burner efficiency varies with the thermal state. The best suited indicator of the engine thermal state is the shaft speed, as it captures transient and static behaviour [34].Thus, a polynomial function of the burner efficiency is achieved though curve fitting of the Figure 8.3.

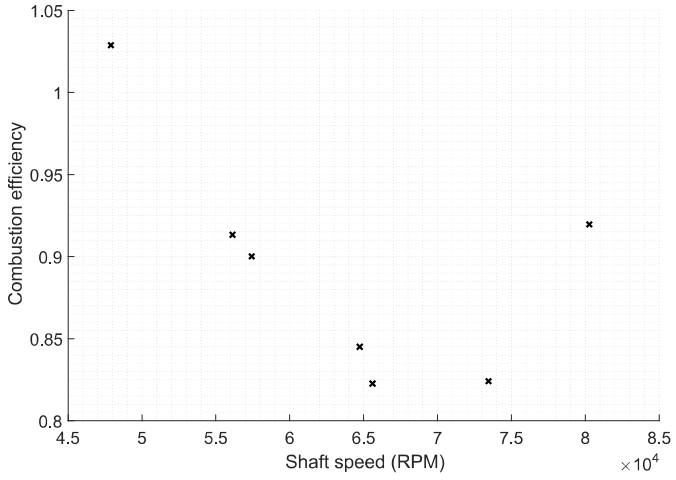

Figure 8.3: Burner efficiency variations through the operation thermal states.

Figure 8.4 shows the pressure loss at different thermal states. As the burner loss is constant, it can be characterized through a static gain, which relates the inlet pressure to the exit pressure by a proportional pressure loss.

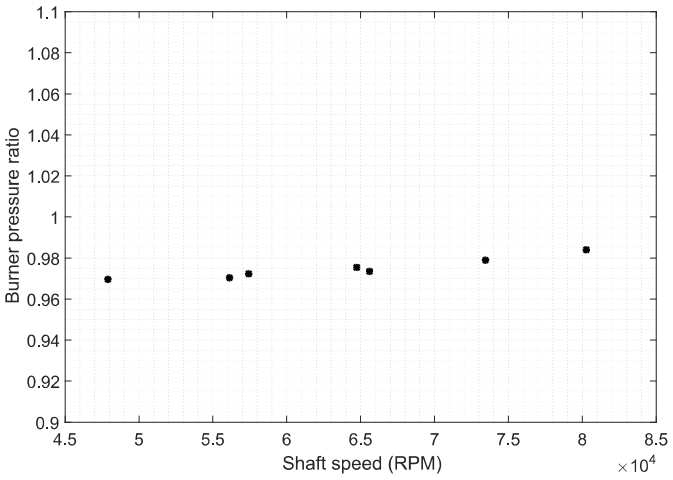

Figure 8.4: Burner efficiency variations through the operation thermal states.

8.3 Nozzle

The nozzle characteristics are represented in the form of ratios. The pressure and temperature vary in small magnitudes with the thermal state of the engine, as presented in the Figure 8.5. Thus, an approximation with dimensionless coefficients is suitable.

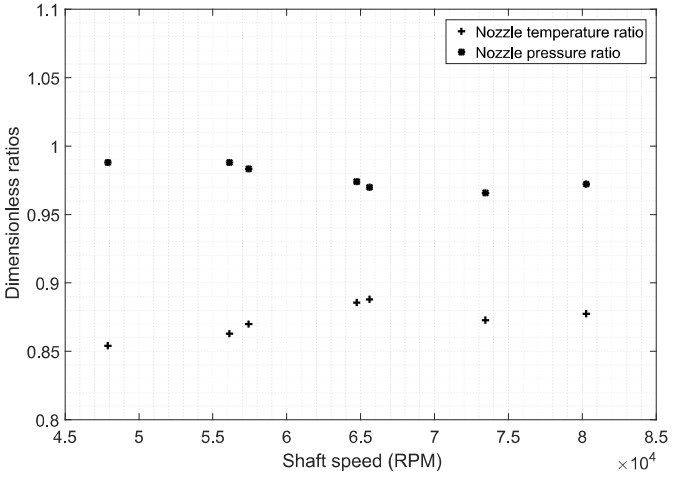

Figure 8.5: Nozzle temperature and pressure ratios.

8.4 Thrust Efficiency

Additional losses are caused by wake loss entropy generation. This is the main loss during jet engine operation and it is dependent on both the operation wind speed and the engine thermal state [1]. Therefore, a thrust efficiency factor is introduced to handle the wake losses. The wind speed effects are integrated in the theoretical thrust computation, thus no extra corrections are required for wind speed operation changes.

$$\eta_T = \frac{T}{T_I} \tag{8.4}$$

8.5 Efficiency parameters

The equations are used to compute the suitable efficiency and dimensionless ratios to model the engine. The value of these parameters is shown in Table 8.1. These values were computed without any wind speed impact from the wind tunnel.

Table 8.1: Micro Turbojet Efficiencies and Dimensionless Ratios

Compressor Work Efficiency	7.01 %
Turbine Work Efficiency	5.84 %
Compressor Polytropic Efficiency	56.34 %
Combustion Chamber Pressure Loss	2.51 %
Nozzle Pressure Ratio	0.97
Nozzle Temperature Ratio	0.85
Thrust Efficiency	98.03 %

The burner efficiency polinomial is:

$$\eta_B = 4.64 * 10^{-8} N^4 - 6.62 * 10^{-4} N^2 + 3.19 \tag{8.5}$$

These parameters are integrated into the block diagram model to estimate the micro turbojet performance with different wind speed and thermal states.

Chapter 9

Validation

The engine was subjected to different operation conditions ranging from 0 to 35 m/s. The wind speed measurements are presented in the Figure 9.1.

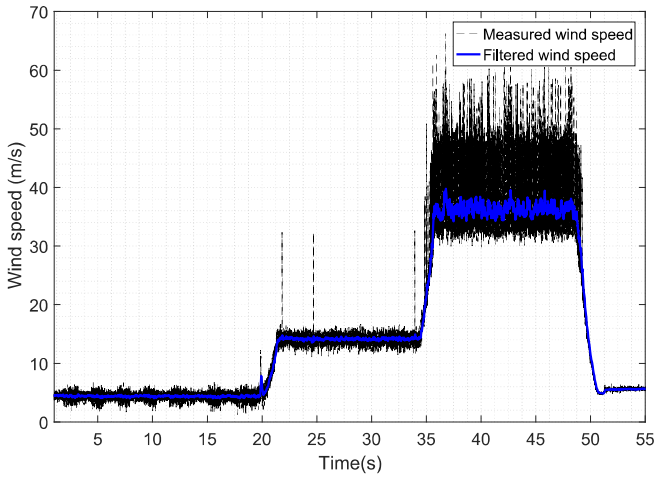

Figure 9.1: Wind measurements for the validation tests.

The main output variable for the model is the thrust. Figure 9.2 shows the identification tests and tests to different wind conditions. The thrust is plotted against test numbers, where each test number corresponds to a different operation condition. Tests 1 to 7 correspond to the identification tests. Used to compute the engine parameters. Test 7 to 13 are engine thrust measurements at different thermal states with no additional wind speed. The tests 14 to 25 are tests at 4.47 m/s, tests

25 to 34 are tests at 14.1 m/s and tests 35 to 46 are tests at 36.3 m/s. The proposed model in this document allows capturing the steady state behaviour of the engine at a full operating regime, whereas conventional aerothermal models are accurate for narrow operation regimes [25].

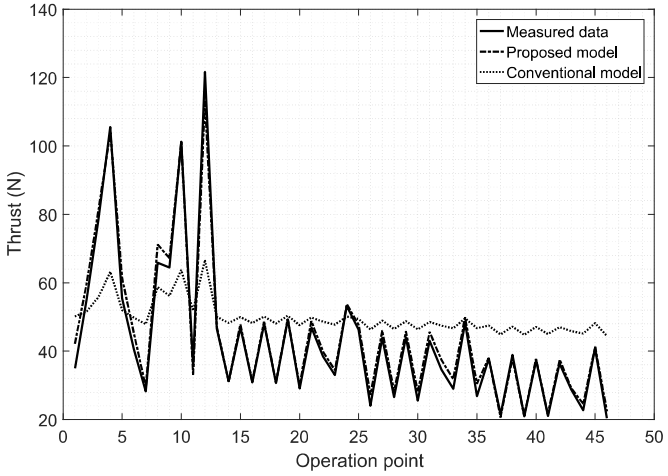

Figure 9.2: Thrust estimation.

The model multivariable estimation capabilities were also tested for the main health indicators. These indicators are the compressor exit pressure, shown in Figure 9.3, and the turbine inlet temperature, presented in Figure 9.4. The pressure estimation is accurate for the whole operation regime, while the turbine inlet temperature loses accuracy at some operating points.

The turbine inlet temperature model inaccuracy is a common problem, where the estimation errors for microturbines can rise up to 200°K [8]. Thus, the proposed model is considered to be accurate for turbine inlet temperature estimation with maximum error below 25°K.

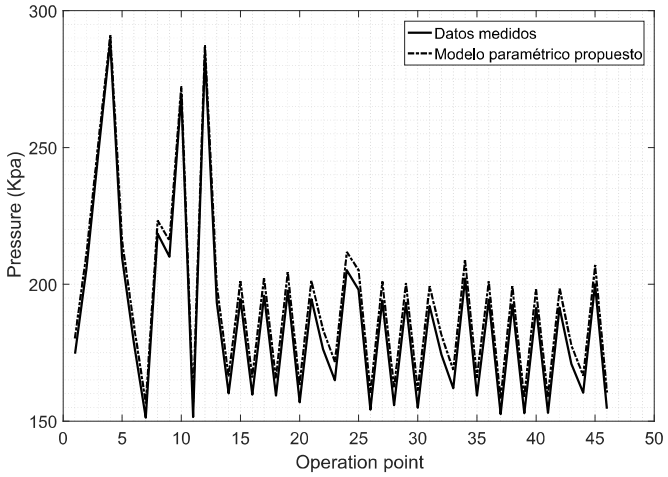

Figure 9.3: Compressor pressure estimation.

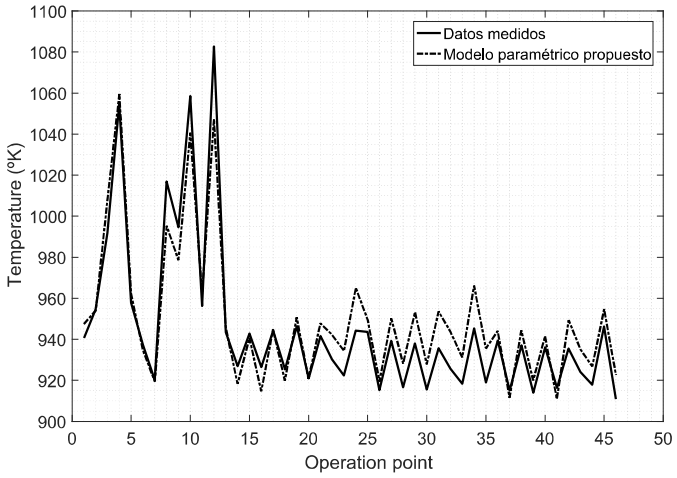

Figure 9.4: Turbine inlet temperature estimation.

Chapter 10

Discussions

The Figure 10.1 presents a deeper analysis of the proposed model thrust estimation accuracy. The proposed model is capable of following the thrust non-linear behaviour through the different operation thermal states with few sensors required for the estimation. The mean average percentile error of the thrust estimation is 6.24 %, which is smaller than the 20% error of the commercial available software and slightly smaller than the 10% error of the estimation through performance map fitting models [23].

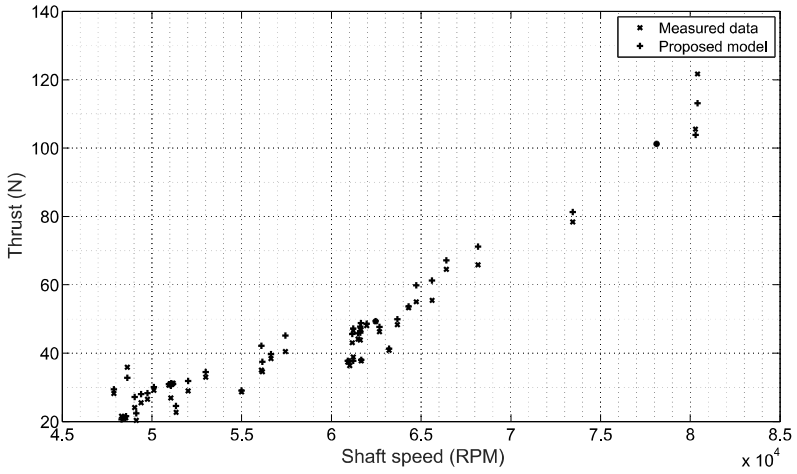

Figure 10.1: Thrust to shaft speed.

The error statistical distribution is analyzed for the estimation of the compres-

sor and exhaust gas temperature. The exit gas temperature is an overall indicator of the engine health degradation [28] and the turbine inlet error can not be adressed as it is one of the inputs for the conventional model. The Figure 10.2 shows that the compressor exit temperature is 112 % more accurate with the proposed model and the error deviation is smaller. For the exhaust gas temperature the error is 66.58 % smaller, although the mean deviation is greater with the proposed model. The errors are compared through the mean average percentile error norm.

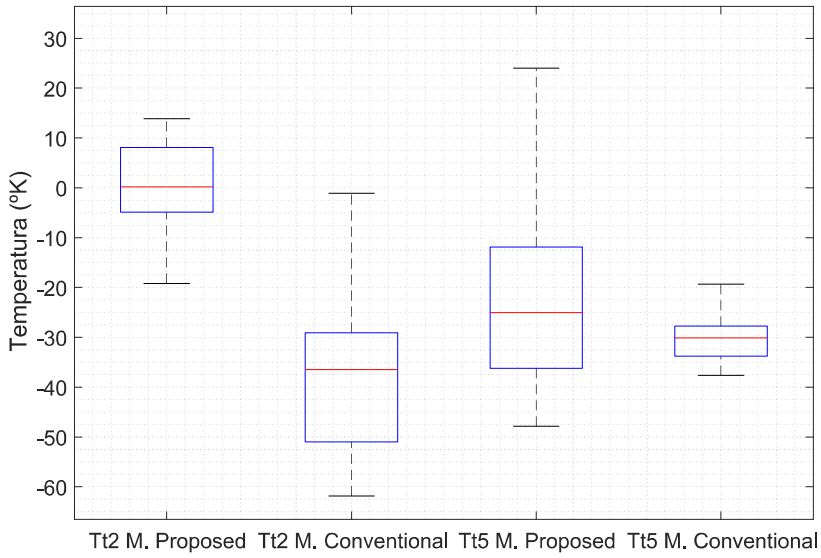

Figure 10.2: Temperature error statistical distribution.

The pressure estimation error distribution is analized for the compressor and nozzle exhaust conditions and presented in the Figure 10.3. The pressure compressor pressure estimation through the proposed model is 36 times more accurate than conventional estimation models, which shows that the developed model is useful as surge margin indicator. The exhaust gas pressure estimation through the proposed model is 35 times more accurate with narrow error distributions.

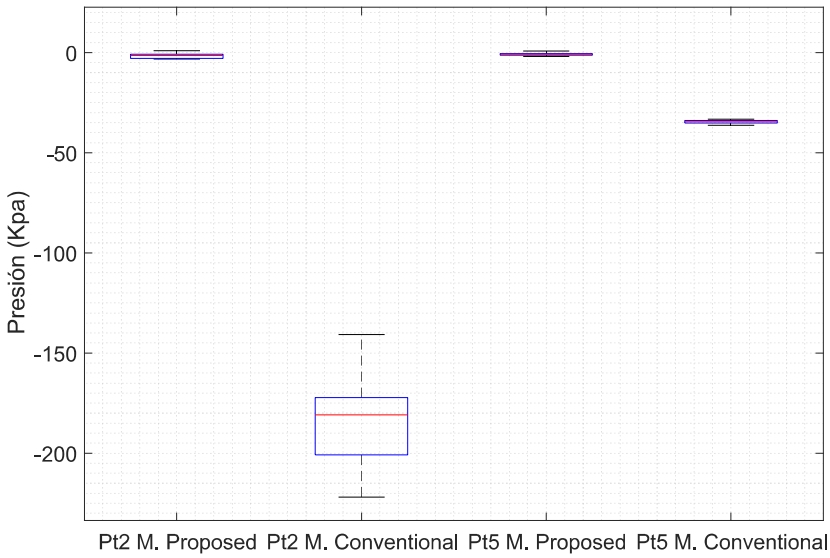

Figure 10.3: Compressor exit pressure error distribution.

Chapter 11

Conclusions

The wind tunnel instrumentation was developed through mass and angular torque conservation. The measurements performed through static pressure sockets capture the wind speed with low cost and simple instrumentation at the cost of high noise and uncertainty in the measurements. The force was measured through a button-type load cell coupled to an elbow to translate angular momentum into force, the captured signal contained stochastic components caused by vibrations and wind turbulence. Thus, signal processing techniques were implemented for the wind speed and aerodynamic drag measurements.

The signals contained a wide spectrum of noise frequencies, in which the process dynamics frequency components can be contained. Autocorrelation functions were implemented to detect any relevant periodic signals due to the high level of uncertainty. However, with the available sensors no oscillatory dynamics were detected. The steady state value of the signals was the variable of interest, a low pass filter was implemented to isolate the static gain components The tests demonstrated that the hysteresis loops are avoided through the implementation of pre-loads. The captured drag coefficient was computed and compared to results of similar experiments. This proved the reliability of the test bench to capture wind speed and force by means of simple non-invasive low cost instrumentation.

Once the test bench is calibrated, the SR-30 engine is installed in the wind tunnel to perform the identification tests. The identification experiments consist of multi-step tests, which are preferred as they contain steady state and dynamic behaviour information. The steady state is obtained by averaging a time window of the measured variables for different operation conditions, characterized by fuel flow (input), shaft speed (thermal state) and free stream properties (wind speed). Thereby, the data was analyzed to provide an insight of the fundamental model structure.

Th fundamental model structure is developed through available engine research, experimental tests and physical laws. The compressor and turbine equations are developed by a combination of modified Euler turbo-machinery equations and energy conservation principles. The combustion chamber behaviour is represented through energy conservation equations, calibrated with a variable burner efficiency to represent the atomization and combustion time variations. The nozzle characteristics were analyzed by means of mass conservation, where experimental data evaluation allowed to simplify the model through static parameters corresponding to temperature and pressure changes. The thrust is computed by a combination of linear momentum and mass conservation principles. The model is submitted to off-identification data tests to prove its accuracy at capturing the micro turbojet fundamental structure.

The engine was submitted to multi-step fuel flow inputs at different free stream wind speeds for its whole operation range. The recorded data of these tests was used only for validation and an additional framework for comparison is developed through the implementation of jet engine theory for larger scale jet engines. The developed model captures the static engine characteristics with higher accuracy than the available theory and commercial software at a wider range of operation conditions. The implementation is compatible with conventional jet engine on-board instrumentation, as few sensors are required.

Bibliography

[1] Abbas, M. y D. W. Riggins, «Exergy-Based Performance Analysis of a Turbojet Engine», en *52nd AIAA/SAE/ASEE Joint Propulsion Conference*, pág. 4638, 2016.

[2] Abdul-Aziz, A., R. D. Bissler y D. B. Stringer, «Turbofan engine performance study under simulated failure and non-traditional flight conditions», en *Smart Materials and Nondestructive Evaluation for Energy Systems IV*, tomo 10601, International Society for Optics and Photonics, pág. 1060106, 2018.

[3] Ailer, P., I. Sinta, G. Szederkényi y K. M. Hangos, «Nonlinear model-building of a low-power gas turbine», *Periodica Polytechnica Transportation Engineering*, **29**(1-2), págs. 117–135, 2001.

[4] Andoga, R., L. Madarasz y L. Fozo, «Intelligent Approaches in Modeling and Control of a Small Turbojet Engines», en *Intelligent Engineering Systems, 2007. INES 2007. 11th International Conference on*, IEEE, págs. 185–190, 2007.

[5] Andrei, I.-C., A. Toader, G. Stroe y F. Frunzulica, «Performance analysis and dynamic modeling of a single-spool turbojet engine», en *AIP Conference Proceedings*, tomo 1798, AIP Publishing, pág. 020005, 2017.

[6] Aretakis, N., I. Roumeliotis, A. Alexiou, C. Romesis y K. Mathioudakis, «Turbofan engine health assessment from flight data», *Journal of Engineering for Gas Turbines and Power*, **137**(4), pág. 041 203, 2015.

[7] ASGARI, H., X. CHEN y R. SAINUDIIN, «Considerations in modelling and control of gas turbines—A review», en *Control, Instrumentation and Automation (ICCIA), 2011 2nd International Conference on*, IEEE, págs. 84–89, 2011.

[8] BADAMI, M., P. NUCCIO y A. SIGNORETTO, «Experimental and numerical analysis of a small-scale turbojet engine», *Energy Conversion and Management*, **76**, págs. 225–233, 2013.

[9] BAKALIS, D. P. y A. G. STAMATIS, «Data analysis and performance model calibration of a small turbojet engine», *Proceedings of the Institution of Mechanical Engineers, Part G: Journal of Aerospace Engineering*, **226**(12), págs. 1523–1533, 2012.

[10] BARLOW, J. B., W. H. RAE y A. POPE, «Low-speed wind tunnel testing», , 1999.

[11] BAUERFEIND, K., «Some general topics in the field of engine handling», *AGARD Eng. Handling 14 p(SEE N 83-29241 18-07)*, 1983.

[12] BAUERFEIND, K., «Technical evaluation report», *AGARD Eng. Handling 7 p(SEE N 83-29241 18-07)*, 1983.

[13] BETTOCCHI, R., P. SPINA y F. FABBRI, «Dynamic modeling of single-shaft industrial gas turbine», en *ASME 1996 International Gas Turbine and Aeroengine Congress and Exhibition*, American Society of Mechanical Engineers, págs. V004T11A007–V004T11A007, 1996.

[14] BORRELL, A., C. EVANS y D. REES, «Identification of aircraft gas turbine dynamics using frequency-domain techniques», , 1998.

[15] BOTROS, A., *Minimizing direct operating cost for turbojet and turboprop aircraft in cruise*, Tesis Doctoral, Concordia University, 2017.

[16] BREIKIN, T., G. KULIKOV, V. ARKOV y P. FLEMING, «Dynamic modelling for condition monitoring of gas turbines: Genetic algorithms approach», *IFAC Proceedings Volumes*, **38**(1), págs. 739–742, 2005.

[17] CATTAFESTA, L., C. BAHR y J. MATHEW, «Fundamentals of wind-tunnel design», *Encyclopedia of Aerospace Engineering*, págs. 1–10, 2010.

[18] ÇENGEL, Y. A., M. A. BOLES y I. A. BUESA, *termodinâmica*, tomo 10, McGraw-Hill São Paulo, 2006.

[19] CHIRAS, N., C. EVANS y D. REES, «Global nonlinear modeling of gas turbine dynamics using NARMAX structures», *Journal of Engineering for Gas Turbines and Power*, **124**(4), págs. 817–826, 2002.

[20] CHIRAS, N., C. EVANS y D. REES, «Nonlinear gas turbine modeling using feedforward neural networks», en *ASME Turbo Expo 2002: Power for Land, Sea, and Air*, American Society of Mechanical Engineers, págs. 145–152, 2002.

[21] CHOWDHURY, H., H. MORIA, A. ALI, I. KHAN, F. ALAM y S. WATKINS, «A study on aerodynamic drag of a semi-trailer truck», *Procedia Engineering*, **56**, págs. 201–205, 2013.

[22] DODD, N. y J. MARTIN, «Using neural networks to optimise gas turbine aero engines», *Computing & Control Engineering Journal*, **8**(3), págs. 129–135, 1997.

[23] ELZAHABY, A. M., M. K. KHALIL y H. E. KHALIL, «Theoretical and Experimental Analysis of a Micro Turbojet Engine's Performance», *International Journal of Scientific & Engineering Research*, **7**(1), págs. 404–410, 2016.

[24] EVANS, C., «Testing and modelling aircraft gas turbines: An introduction and overview», , 1998.

[25] EVANS, C., «Testing and modelling aircraft gas turbines: An introduction and overview», , 1998.

[26] EVANS, D., D. REES y D. JONES, «Identifying linear models of systems suffering nonlinear distortions, with a gas turbine application», *IEE Proceedings-Control Theory and Applications*, **142**(3), págs. 229–240, 1995.

[27] GLASS, J. W., «NARMAX modelling and robust control of internal combustion engines», *International Journal of Control*, **72**(4), págs. 289–304, 1999.

[28] HANACHI, H., J. LIU, A. BANERJEE, Y. CHEN y A. KOUL, «A physics-based modeling approach for performance monitoring in gas turbine engines», *IEEE Transactions on Reliability*, **64**(1), págs. 197–205, 2015.

[29] HILL, D. C., «Identification of gas turbine dynamics: time-domain estimation problems», en *ASME 1997 International Gas Turbine and Aeroengine Congress and Exhibition*, American Society of Mechanical Engineers, págs. V004T15A008–V004T15A008, 1997.

[30] HSIA, T. C., *System identification: least-squares methods*, tomo 1, Lexington books Lexington, 1977.

[31] HÜNECKE, K., *Jet engines: Fundamentals of theory, design and operation*, Airlife, 1997.

[32] KLEIN, D. y C. ABEYKOON, «Modelling of a turbojet gas turbine engine», en *Internet Technologies and Applications (ITA), 2015*, IEEE, págs. 200–206, 2015.

[33] KOIKE M., N. T. Y. H. N., «Mitsubishi motors technical review», **16**(11), pág. 11, 2004.

[34] KOMJÁTY, M., L. FŐZŐ y R. ANDOGA, «Experimental identification of a small turbojet engine with variable exhaust nozzle», en *2015 16th IEEE International Symposium on Computational Intelligence and Informatics (CINTI)*, IEEE, págs. 65–69, 2015.

[35] KRISHNAKUMAR, K., Y. YACHISAKO y Y. HUANG, «Jet engine performance estimation using intelligent system technologies», en *39th Aerospace Sciences Meeting and Exhibit*, pág. 1122, 2001.

[36] KRISHNAKUMAR, K., Y. YACHISAKO y Y. HUANG, «Jet engine performance estimation using intelligent system technologies», en *39th Aerospace Sciences Meeting and Exhibit*, pág. 1122, 2001.

[37] KULIKOV, G. G. y H. A. THOMPSON, *Dynamic modelling of gas turbines: identification, simulation, condition monitoring and optimal control*, Springer Science & Business Media, 2013.

[38] LEFEBVRE, A. H. y D. R. BALLAL, *Gas turbine combustion: alternative fuels and emissions*, CRC press, 2010.

[39] LÉONARD, O., S. BORGUET y P. DEWALLEF, «Adaptive estimation algorithm for aircraft engine performance monitoring», *Journal of Propulsion and Power*, **24**(4), págs. 763–769, 2008.

[40] LÉONARD, O., J. THOMAS y S. BORGUET, «Ten years of Experience with a Small Jet Engine as a Support for Education», *Journal of Engineering for Gas Turbines and Power*, **131**(1), pág. 012 303, 2009.

[41] LI, Y. y T. KORAKIANTIS, «Nonlinear weighted-least-squares estimation approach for gas-turbine diagnostic applications», *Journal of Propulsion and Power*, **27**(2), págs. 337–345, 2011.

[42] LICHTSINDER, M. y Y. LEVY, «Jet engine model for control and real-time simulations», *Journal of Engineering for Gas Turbines and Power*, **128**(4), págs. 745–753, 2006.

[43] LIU, X. y L. ZHAO, «Approximate nonlinear modeling of aircraft engine surge margin based on equilibrium manifold expansion», *Acta Aeronautica et Astronautica Sinica*, **25**(5), págs. 663–674, 2012.

[44] LYANTSEV, O., A. KAZANTSEV y A. ABDULNAGIMOV, «Identification method for nonlinear dynamic models of gas turbine engines on acceleration mode», *Procedia Engineering*, **176**, págs. 409–415, 2017.

[45] MARTIN, S., I. WALLACE y D. G. BATES, «Development and validation of an aero-engine simulation model for advanced controller design», en *American Control Conference, 2008*, IEEE, págs. 2334–2339, 2008.

[46] MATTINGLY, J. D., *Elements of propulsion: gas turbines and rockets*, American Institute of Aeronautics and Astronautics, 2006.

[47] MOHAMMADI, E. y M. MONTAZERI-GH, «A new approach to the gray-box identification of wiener models with the application of gas turbine engine modeling», *Journal of Engineering for Gas Turbines and Power*, **137**(7), pág. 071 202, 2015.

[48] MOYES, S., «Principles of Jet Propulsion and Gas Turbines», *Nature*, **164**(4162), pág. 202, 1949.

[49] MU, J. y D. REES, «Approximate model predictive control for gas turbine engines», en *American Control Conference, 2004. Proceedings of the 2004*, tomo 6, IEEE, págs. 5704–5709, 2004.

[50] NAYYERI, H. y K. KHORASANI, «Modeling aircraft jet engine and system identification by using genetic programming», en *Electrical & Computer Engineering (CCECE), 2012 25th IEEE Canadian Conference on*, IEEE, págs. 1–4, 2012.

[51] OELBERG, E. y L. RODRIGUES, «Maximum Endurance of a Turbofan in Cruise with Head or Tail-Wind», en *2018 Annual American Control Conference (ACC)*, IEEE, págs. 2270–2275, 2018.

[52] ONIONS, R. y A. FOSS, «Improvements in the dynamic simulation of gas turbines», *AGARD Eng. Handling 16 p(SEE N 83-29241 18-07)*, 1983.

[53] PANOV, V., «Gas turbine performance diagnostics and fault isolation based on multidimensional complex health vector space», en *ETC2015-0051, 11th European Turbomachinery Conference, Madrid, Spain*, págs. 23–27, 2015.

[54] POURMOVAHED, A., C. JERUZAL y K. BRINKER, «Development of a jet engine experiment for the energy systems laboratory», en *ASME 2003 International Mechanical Engineering Congress and Exposition*, American Society of Mechanical Engineers, págs. 229–247, 2003.

[55] RUANO, A. E., P. J. FLEMING, C. TEIXEIRA, K. RODRIGUEZ-VÁZQUEZ y C. M. FONSECA, «Nonlinear identification of aircraft gas-turbine dynamics», *Neurocomputing*, **55**(3-4), págs. 551–579, 2003.

[56] SKRUCANY, T., B. SARKAN y J. GNAP, «Influence of aerodynamic trailer devices on drag reduction measured in a wind tunnel», *Eksploatacja i Niezawodność*, **18**(1), 2016.

[57] SLAVICA, R., «Flow Visualization Techniques in Wind Tunnels Part I-Non optical Methods», *Scientific Technical Review, Vol. LV II*, **1**, págs. 39–50, 2007.

[58] SUGIYAMA, N., «System identification of jet engines», en *ASME 1998 International Gas Turbine and Aeroengine Congress and Exhibition*, American Society of Mechanical Engineers, págs. V005T15A007–V005T15A007, 1998.

[59] TAGASHIRA, T., N. SUGIYAMA y M. KOH, «Dynamic Characteristic Tests of Single Spool Turbojet Engine Using Altitude Test Facility», en *43rd AIAA/ASME/SAE/ASEE Joint Propulsion Conference & Exhibit*, pág. 5012, 2007.

[60] TAVAKOLPOUR-SALEH, A., S. NASIB, A. SEPASYAN y S. HASHEMI, «Parametric and nonparametric system identification of an experimental turbojet engine», *Aerospace Science and Technology*, **43**, págs. 21–29, 2015.

[61] TESAŘ, V., «Characterisation of subsonic axisymmetric nozzles», *Chemical Engineering Research and Design*, **86**(11), págs. 1253–1262, 2008.

[62] TORRES, M. P., G. SOSA, L. AMEZQUITA-BROOKS, E. LICEAGA-CASTRO y P. DEL C ZAMBRANO-ROBLEDO, «Identification of the fuel-thrust dynamics of

a gas turbo engine», en *Decision and Control (CDC), 2013 IEEE 52nd Annual Conference on*, IEEE, págs. 4535–4540, 2013.

[63] TSOUTSANIS, E., Y.-G. LI, P. PILIDIS y M. NEWBY, «Non-linear model calibration for off-design performance prediction of gas turbines with experimental data», *The Aeronautical Journal*, **121**(1245), págs. 1758–1777, 2017.

[64] TSOUTSANIS, E., N. MESKIN, M. BENAMMAR y K. KHORASANI, «An efficient component map generation method for prediction of gas turbine performance», en *ASME Turbo Expo 2014: Turbine Technical Conference and Exposition*, American Society of Mechanical Engineers, págs. V006T06A006–V006T06A006, 2014.

[65] TSOUTSANIS, E., N. MESKIN, M. BENAMMAR y K. KHORASANI, «Transient gas turbine performance diagnostics through nonlinear adaptation of compressor and turbine maps», *Journal of Engineering for Gas Turbines and Power*, **137**(9), pág. 091 201, 2015.

[66] TURNS, S. R. *et al.*, *An introduction to combustion*, tomo 499, McGraw-hill New York, 1996.

[67] VILLARREAL VALDERRAMA, F., L. AMÉZQUITA BROOKS, D. MARTÍNEZ LIBRADO y J. Y. LICEAGA CASTRO, E, «Banco de pruebas no invasivas para caracterización de arrastre aerodinámico: aplicación en turborreactor SR-30.», .

[68] VYAS, U., V. ANDREOLI y G. PANIAGUA, «Effect of transonic inlet design on the performance of a mico-turbojet engine», en *2018 AIAA Aerospace Sciences Meeting*, pág. 1624, 2018.

[69] WARHAFT, Z., «The engine and the atmosphere: An introduction to engineering», , 1998.

[70] WOOD, R. M. y S. X. BAUER, «Simple and low-cost aerodynamic drag reduction devices for tractor-trailer trucks», *Informe técnico*, SAE Technical Paper, 2003.

[71] YADAV, R., Y. KAPADI y A. PASHILKAR, «Aero-thermodynamic model for digital simulation of turbofan engine», en *ASME Turbo Expo 2005: Power for Land, Sea, and Air*, American Society of Mechanical Engineers, págs. 63–70, 2005.

[72] YARLAGADDA, S., *Performance analysis of J85 turbojet engine matching thrust with reduced inlet pressure to the compressor*, Tesis Doctoral, University of Toledo, 2010.

[73] YAZAR, I., H. S. YAVUZ y A. A. YAVUZ, «Comparison of various regression models for predicting compressor and turbine performance parameters», *Energy*, **140**, págs. 1398–1406, 2017.

[74] YU, D., H. ZHAO, Z. XU, Y. SUI y J. LIU, «An approximate non-linear model for aeroengine control», *Proceedings of the Institution of Mechanical Engineers, Part G: Journal of Aerospace Engineering*, **225**(12), págs. 1366–1381, 2011.

[75] YU, H., Y. YUECHENG, Z. SHIYING y S. ZHENSHENG, «Comparison of linear models for gas turbine performance», *Proceedings of the Institution of Mechanical Engineers, Part G: Journal of Aerospace Engineering*, **228**(8), págs. 1291–1301, 2014.

[76] ZHAO, Y.-P., Q.-K. HU, J.-G. XU, B. LI, G. HUANG y Y.-T. PAN, «A robust extreme learning machine for modeling a small-scale turbojet engine», *Applied Energy*, **218**, págs. 22–35, 2018.

Autobiography

Jose Francisco Villarreal Valderrama

Candidate to obtain the degree of
Maestría en Ingeniería Aeronáutica
con orientacion en Dinámica de Vuelo

Universidad Autónoma de Nuevo León
Facultad de Ingeniería Mecánica y Eléctrica

Thesis:
Analysis and modeling of micro turbojets: a comprehensive model based on multiphysics principles

Born in Monterrey, Nuevo León on May 22 at the year of 1995. His parents are José Francisco Villarreal Lozano and Virginia Valderrama Almanza. Graduated in Aeronautical Engineering on July 2017, from the Facultad de Ingeniería Mecánica y Eléctrica.